Table 1. Reported cases of anti-p200 pemphigoid in the English-language literature

Patient No.	Age, years/sex	Clinical features	Detected antigen	IIF titer	Treatment	Scar formation
1 [1]	72/F	BP-like	200/230	1:160	Cyclosporine	–
2 [2]	54/M	BP-like	200	1:80	TC, colchicine	–
3 [17]	31/F	BP-like	200/210	1:10	Topical steroid	–
4 [8]	64/M	DH-like	180/200		Systemic steroid	–
5 [10]	72/M	LABD-like	200		DDS	–
6 [16]	64/M	Vesicular pemphigoid-like	200		Systemic steroid, DDS	–
7 [16]	64/M	Vesicular pemphigoid-like	200		Systemic steroid, DDS	–
8 [7]	81/M	BP-like	200		TC, NA	–
9 [14]	69/M	BP-like	200/230		MINO	–
10 [14]	70/M	BP-like	200		TC, NA, systemic steroid	–
11 [14]	54/M	BP-like	200		Cyclosporine	–
12 [14]	76/M	BP-like	200/230		Systemic steroid	–
13 [5]	52/M	BP-like	200	1:40	Topical steroid	–
14 [6]	61/M	BP-like	200	1:40	Systemic steroid, DDS	–
15 [11]	66/F	LABD-like	200	1:160	Systemic steroid, TC, DDS, plasmapheresis	–
16 [13]	51/M	BP-like, LABD-like	200/260	1:400	Systemic steroid, IVIG, DDS, steroid pulse mycophenolate mofetil	–
17 [12]	28/M	LABD-like	200	1:160	Systemic steroid, azathioprine	+
18 [35]	49/M	BP-like	200		Systemic steroid, DDS	–
19 [28]	29/F	Vesicular pemphigoid-like	200/290	1:160	Systemic steroid, MINO, NA, steroid pulse	–
20 [9]	75/M	DH-like	200		Systemic steroid, cyclosporine	–
21 [3]	56/F	Pompholyx-like	165/200 (α_3-subunit of laminin 5)	1:80	Systemic steroid, azathioprine	–
22 [29]	52/F	BP-like	200/290	1:32	Systemic steroid	+
23 [15]	17/F	BP-like	200	1:320	Systemic steroid, DDS	+
24 [36]	84/M		200			–
25 [36]	91/F		200			–
26 [36]	50/M		200			–
27 [36]	74/M		200			–
28 [26]	65/M	EBA-like	200/290		Systemic steroid, DDS, cyclosporine, mycophenolate mofetil, IVIG	+
29 [18]	61/M	BP-like	200	1:20	Systemic steroid, DDS	–
30 [18]	45/M		200		Topical steroid	–
31 [18]	Young boy		200			
32 [27]	64/F	ALMMP-like	200/γ_2-subunit of laminin 5		Steroid, MINO, IVIG	+
Present case	53/F	LABD-like	180/200	>640-fold dilution	Systemic steroid, MINO, NA, steroid pulse	+

BP = Bullous pemphigoid; DH = dermatitis herpetiformis; LABD = linear IgA bullous dermatosis; EBA = epidermolysis bullosa acquisita; ALMMP = antilaminin 5 mucous membrane pemphigoid; IIF = indirect immunofluorescence; TC = tetracycline; DDS = dapsone; NA = nicotinamide; MINO = minocycline; IVIG = intravenous immunoglobulin.

therapy might, therefore, be effective for severe and refractory anti-p200 pemphigoid cases.

Interestingly, this case also had IgG autoantibodies directed against Col17 present. Coexistence of autoantibodies other than anti-p200 autoantigen in anti-p200 pemphigoid is uncommon, but cases with autoantibodies to the α_3-chain of laminin 5 [3], the γ_2-subunit of laminin 5 [27] and type VII collagen [28, 29] have been reported (table 1). There has been only 1 case reported previously in which autoantibodies to both Col17 and p200 autoantigen were detected (table 1) [8]. In autoimmune diseases, it is well known that autoantibodies of patients in the later disease stages are more likely to react with multiple sites of autoantigens than those of patients in early stages of the disease. This is known as 'epitope spreading' [30–32]. However, in

our case, IgG autoantibodies against Col17 could already be detected from the very early stages when the patient initially presented at our clinic. IgG autoantibodies in bullous pemphigoid patients have been reported to be directly pathogenic as they are able to induce separation of the dermis and epidermis in vitro [33]. In addition, IgG autoantibodies directed against the NC16A domain in Col17 from bullous pemphigoid patients have recently been reported to be able to induce detachment of the dermis and epidermis in vivo in a Col17-humanized mouse model [34]. Taken together, we have to assume that autoantibodies to Col17 in the present case, such as those in bullous pemphigoid patients, might also contribute to blister formation, and may also be related to the severity seen in this case.

Acknowledgements

We thank Dr. James R. McMillan and Heather Ann Long for their kind help with English-language editing and proofreading.

References

1 Chen KR, Shimizu S, Miyakawa S, Ishiko A, Shimizu H, Hashimoto T: Coexistence of psoriasis and an unusual IgG-mediated subepidermal bullous dermatosis: identification of a novel 200-kDa lower lamina lucida target antigen. Br J Dermatol 1996;134:340–346.
2 Zillikens D, Kawahara Y, Ishiko A, Shimizu H, Mayer J, Rank CV, Liu Z, Giudice GJ, Tran HH, Marinkovich MP, Brocker EB, Hashimoto T: A novel subepidermal blistering disease with autoantibodies to a 200-kDa antigen of the basement membrane zone. J Invest Dermatol 1996;106:465–470.
3 Shimanovich I, Petersen EE, Weyers W, Sitaru C, Zillikens D: Subepidermal blistering disease with autoantibodies to both the p200 autoantigen and the α3 chain of laminin 5. J Am Acad Dermatol 2005;52:S90–S92.
4 Amrei D, Christian R, Takashi H, Zillikens D, Shimanovich I: Anti-p200 pemphigoid: a novel autoimmune subepidermal blistering disease. J Dermatol 2007;34:1–8.
5 Zillikens D, Ishiko A, Jonkman MF, Chimanovitch I, Shimizu H, Hashimoto T, Brocker EB: Autoantibodies in anti-p200 pemphigoid stain skin lacking laminin 5 and type VII collagen. Br J Dermatol 2000;143:1043–1049.
6 Egan CA, Yee C, Zillikens D, Yancey KB: Anti-p200 pemphigoid: diagnosis and treatment of a case presenting as an inflammatory subepidermal blistering disease. J Am Acad Dermatol 2002;46:786–789.
7 Mascaro JM Jr, Zillikens D, Giudice GJ, Caux F, Fleming MG, Katz HM, Diaz LA: A subepidermal bullous eruption associated with IgG autoantibodies to a 200 kD dermal antigen: the first case report from the United States. J Am Acad Dermatol 2000;42:309–315.
8 Salmhofer W, Kawahara Y, Soyer HP, Kerl H, Nishikawa T, Hashimoto T: A subepidermal blistering disease with histopathological features of dermatitis herpetiformis and immunofluorescence characteristics of bullous pemphigoid: a novel subepidermal blistering disease or a variant of bullous pemphigoid? Br J Dermatol 1997;137:599–604.
9 Yasuda H, Tomita Y, Shibaki A, Hashimoto T: Two cases of subepidermal blistering disease with anti-p200 or 180-kD bullous pemphigoid antigen associated with psoriasis. Dermatology 2004;209:149–155.
10 Kawahara Y, Matsuo Y, Hashimoto T, Nishikawa T: A case of unique subepidermal blistering disease with autoantibodies against a novel dermal 200-kD antigen. Dermatology 1998;139:738–759.
11 Watanabe M, Tsunoda T, Tagami H: A subepidermal blistering dermatosis associated with coexistent IgG and IgA anti-dermal basement membrane zone antibodies: demonstration of IgG antibodies reactive against a 200-kDa dermal antigen. Eur J Dermatol 2002;12:603–606.
12 Umemoto N, Demitsu T, Toda S, Noguchi T, Suzuki SI, Kakurai M, Yamada T, Suzuki M, Nakagawa H, Komai A, Hashimoto T: A case of anti-p200 pemphigoid clinically mimicking inflammatory epidermolysis bullosa acquisita. Br J Dermatol 2003;148:1058–1059.
13 Morris SD, Mallipeddi R, Oyama N, Gratian MJ, Harman KE, Bhogal BS, Black MM, Eady RA, Hashimoto T, McGrath JA: Psoriasis bullosa acquisita. Clin Exp Dermatol 2002;27:665–669.
14 Kawahara Y, Zillikens D, Yancy KB, Marinkovich MP, Nie Z, Hashimoto T, Nishikawa T: Subepidermal blistering disease with autoantibodies against a novel dermal 200-kD antigen. J Dermatol Sci 2000;23:93–102.
15 Yamane N, Sawamura D, Nishie W, Abe M, Kodama K, Adachi K, Nakamura H, Ishii N, Hashimoto T, Shimizu H: Anti-p200 pemphigoid in a 17-year-old girl successfully treated with systemic corticosteroid and dapsone. Br J Dermatol 2007;156:1075–1078.
16 Inoh Y, Nishikawa T, Hashimoto T: The vesicular pemphigoid phenotype may be related to antibodies to a 200-kDa antigen in the lower lamina lucida. Br J Dermatol 1998;139:738–759.
17 Saeki H, Hayashi N, Komine N, Soma Y, Shimada S, Watanabe K, Hasimoto T: A case of generalized pustular psoriasis followed by bullous disease: an atypical case of bullous pemphigoid or a novel bullous disease? Br J Dermatol 1996;134:152–155.
18 Hofmann SC, Voith U, Sasaki T, Trueb RM, Nischt R, Bruckner-Tuderman L: The autoantigen in anti-p200 pemphigoid is synthesized by keratinocytes and fibroblasts and is distinct from nidogen-2. J Invest Dermatol 2008;128:87–95.
19 Tsuji Y, Kawashima T, Yokota K, Tateishi Y, Tomita Y, Matsumura T, Shimizu H: Clinical and serological transition from pemphigus vulgaris to pemphigus foliaceus demonstrated by desmoglein ELISA system. Arch Dermatol 2002;138:95–96.
20 Tsuji-Abe Y, Akiyama M, Yamanaka Y, Kikuchi T, Sato-Matsumura KC, Shimizu H: Correlation of clinical severity and ELISA indices for the NC16A domain of BP180 measured using BP180 ELISA kit in bullous pemphigoid. J Dermatol Sci 2005;37:145–149.
21 Schmidt E, Obe K, Brocker EB, Zillikens D: Serum levels of autoantibodies to BP180 correlate with disease activity in patients with bullous pemphigoid. Arch Dermatol 2000;136:174–178.
22 Wojnarowska F, Venning VA, Burge SM: Immunobullous diseases; in Burns T, Breathnach S, Cox N, Griffiths C (eds): Rook's Textbook of Dermatology, ed 7. Oxford, Blackwell, 2004, vol 2, pp 41.1–41.59.
23 Fleming TE, Korman NJ: Cicatricial pemphigoid. J Am Acad Dermatol 2000;43:571–591.
24 Engineer L, Ahmed AR: Emerging treatment for epidermolysis bullosa acquisita. J Am Acad Dermatol 2001;44:818–828.
25 Bedane C, McMillan JR, Balsding SD, Bernard P, Prost C, Bonnetblanc JM, Diaz LA, Eady RA, Giudice GJ: Bullous pemphigoid and cicatricial pemphigoid autoantibodies react with ultrastructurally separable epitopes on the BP180 ectodomain: evidence that BP180 spans the lamina lucida. J Invest Dermatol 1997;108:901–907.

26 Pastar Z, Rados J, Lipozencic J, Dobric I, Marinovic B, Ishii N, Hashimoto T: Case of concurrent epidermolysis bullosa acquisita and anti-p200 pemphigoid: how to treat it? Int J Dermatol 2007;46:295–298.
27 Mitsuya J, Hara H, Ito K, Ishii N, Hashimoto T, Terui T: Metastatic ovarian carcinoma-associated subepidermal blistering disease with autoantibodies to both the p200 dermal antigen and the gamma 2 subunit of laminin 5 showing unusual clinical features. Br J Dermatol 2008;158:1354–1357.
28 Furukawa H, Miura T, Takahashi M, Nakamura K, Kaneko F, Ishii F, Komai R, Hashimoto T: A case of anti-p200 pemphigoid with autoantibodies against both a novel 200-kD dermal antigen and the 290-kD epidermolysis bullosa acquisita antigen. Dermatology 2004;209:145–148.
29 Yamada T, Suzuki M, Koike Y, Kida K, Murata S, Hashimoto T, Ohtsuki M: A case of epidermolysis bullosa acquisita with autoantibody to anti-p200 pemphigoid antigen and exfoliative esophagitis. Dermatology 2006; 212:381–384.
30 Fairley JA, Woodley DT, Chen M, Giudice GJ, Lin MS: A patient with both bullous pemphigoid and epidermolysis bullosa acquisita: an example of intermolecular epitope spreading. J Am Acad Dermatol 2004;51:118–122.
31 Maeda JY, Moura AK, Maruta CW, Santi CG, Prisayanh PS, Aoki V: Changes in the autoimmune blistering response: a clinical and immunopathological shift from pemphigus foliaceus to bullous pemphigoid. Clin Exp Dermatol 2006;31:653–655.
32 Peterson JD, Chang AJ, Chan LS: Clinical evidence of an intermolecular epitope spreading in a patient with pemphigus foliaceus converting into bullous pemphigoid. Arch Dermatol 2007;143:272–274.
33 Sitaru C, Schmidt E, Petermann S, Munteanu LS, Brocker EB, Zillikens D: Autoantibodies to bullous pemphigoid antigen 180 induce dermal-epidermal separation in cryosections of human skin. J Invest Dermatol 2002;118:664–671.
34 Nishie W, Sawamura D, Goto M, Ito K, Shibaki A, McMillan JR, Sakai K, Nakamura H, Olasz E, Yancey KB, Akiyama M, Shimizu H: Humanization of autoantigen. Nat Med 2007;13:378–383.
35 Cho SB, Kim SC: A Korean case of anti-p200 pemphigoid. Yonsei Med J 2003;44:931–934.
36 Rose C, Weyers W, Denisjuk N, Hillen U, Zillikens D, Shimanovich I: Histopathology of anti-p200 pemphigoid. Am J Dermatopathol 2007;29:119–124.

Immunological Reconstitution after Autologous Hematopoietic Stem Cell Transplantation in Patients with Systemic Sclerosis: Relationship Between Clinical Benefits and Intensity of Immunosuppression

TOSHIYUKI BOHGAKI, TATSUYA ATSUMI, MIYUKI BOHGAKI, AKIRA FURUSAKI, MAKOTO KONDO, KAZUKO C. SATO-MATSUMURA, RIICHIRO ABE, HIROSHI KATAOKA, TETSUYA HORITA, SHINSUKE YASUDA, YOSHIHARU AMASAKI, MITSUFUMI NISHIO, KEN-ICHI SAWADA, HIROSHI SHIMIZU, and TAKAO KOIKE

ABSTRACT. ***Objective.*** To analyze the relationship between clinical benefits and immunological changes in patients with systemic sclerosis (SSc) treated with autologous hematopoietic stem cell transplantation (HSCT).

Methods. Ten patients with SSc were treated with high-dose cyclophosphamide followed by highly purified CD34+ cells (n = 5) or unpurified grafts (n = 5). Two groups of patients were retrospectively constituted based on their clinical response (good responders, n = 7; and poor responders, n = 3). As well as clinical findings, immunological reconstitution through autologous HSCT was assessed by fluorescence-activated cell sorter analysis, quantification of signal joint T cell receptor rearrangement excision circles (sjTREC), reflecting the thymic function, and *foxp3*, a key gene of regulatory T cells, mRNA levels.

Results. Patients' clinical and immunological findings were similar between good and poor responders, or CD34-purified and unpurified groups at inclusion. The sjTREC values were significantly suppressed at 3 months after autologous HSCT in good responders compared with poor responders ($p = 0.0152$). Reconstitution of CD4+CD45RO- naive T cells was delayed in good responders compared with poor responders. The phenotype of other lymphocytes, cytokine production in T cells, and *foxp3* gene expression levels after autologous HSCT did not correlate with clinical response in good or poor responders. Clinical and immunological findings after autologous HSCT were similar between CD34-purified and unpurified groups.

Conclusion. Our results suggest that immunosuppression intensity, sufficient to induce transient suppression of thymic function, is attributable to the feasible clinical response in patients with SSc treated with autologous HSCT. Appropriate monitoring of sjTREC values may predict clinical benefits in transplanted SSc patients after autologous HSCT. (First Release May 15 2009; J Rheumatol 2009;36:1240–8; doi:10.3899/jrheum.081025)

Key Indexing Terms:
SYSTEMIC SCLEROSIS HEMATOPOIETIC STEM CELL TRANSPLANTATION
IMMUNOLOGICAL RECONSTITUTION

From the Department of Medicine II and the Department of Dermatology, Hokkaido University Graduate School of Medicine, Sapporo; and Third Department of Internal Medicine, Akita University School of Medicine, Akita, Japan.

Supported by a grant from the Japanese Ministry of Health, Labor and Welfare.

T. Bohgaki, MD, PhD; T. Atsumi, MD, PhD; M. Bohgaki, MD, PhD; A. Furusaki, MD, PhD; M. Kondo, MD, PhD, Department of Medicine II; K.C. Sato-Matsumura, MD, PhD; R. Abe, MD, PhD, Department of Dermatology; H. Kataoka, MD, PhD; T. Horita, MD, PhD; S. Yasuda, MD, PhD; Y. Amasaki, MD, PhD; M. Nishio, MD, PhD, Department of Medicine II, Hokkaido University Graduate School of Medicine; K. Sawada, MD, PhD, Third Department of Internal Medicine, Akita University School of Medicine; H. Shimizu, MD, PhD, Department of Dermatology; T. Koike, MD, PhD, Department of Medicine II, Hokkaido University School of Medicine.

Address reprint requests to Dr. T. Atsumi, Department of Medicine II, Hokkaido University Graduate School of Medicine, N15, W7, Kita-ku, Sapporo 060-8638, Japan. E-mail: at3tat@med.hokudai.ac.jp

Accepted for publication January 8, 2009.

Systemic sclerosis (SSc) is an autoimmune disease characterized by the presence of skin sclerosis, organ fibrosis, and autoantibodies[1]. Despite extensive research on autoimmunology and endotheliology, its pathophysiology has been far from conclusive[2,3]. The skin and organ manifestations of SSc are, in general, slowly progressive and chronically disabling. In some patients, however, they can be rapidly progressive and fatal due to organ involvements such as interstitial pneumonia, arrhythmia, and renal failure. Severe organ involvement frequently occurs within the first 3 years of disease[1]. These clinical features affect daily living activity and life expectancy in patients with SSc.

Autologous hematopoietic stem cell transplantation (HSCT) has been indicated for patients with autoimmune diseases, resulting in great success particularly in patients with SSc[4-10]. Autologous HSCT is one of the treatments in

Personal non-commercial use only. The Journal of Rheumatology Copyright © 2009. All rights reserved.

patients suffering from hematological malignant diseases. For the practice of autologous HSCT against those malignant diseases, graft manipulation using antibody specific for CD34, a marker of human hematopoietic stem cells, is usually essential to deplete malignant cells from the graft. On the other hand, patients treated with CD34+-selected autologous HSCT (CD34-HSCT) may have infectious complications during hematological recovery more frequently than patients treated with unselected autologous HSCT (unselected-HSCT)[11]. The graft manipulation was performed in many patients with severe autoimmune diseases treated by autologous HSCT in consideration of depleting autoreactive lymphocytes and inducing profound clinical remission. Meanwhile, it has been debated whether CD34+ cell selection in the graft is necessary or not[9,12].

The difference in conditioning regimens is not related to the clinical benefits, and about one-third of transplanted patients do not benefit from these intensive immunosuppressive treatment[9,13]. Clinical response may depend on profound qualitative immunological changes obtained by autologous HSCT in patients with systemic lupus erythematosus or multiple sclerosis[14,15]. Little is known as to why and how patients with SSc have clinical benefits of autologous HSCT. The aim of our study was to elucidate the relationship between clinical effect and alteration of immunological profiles in patients with SSc treated with autologous HSCT.

MATERIALS AND METHODS

Patients. Our study was approved by the ethical committee of Hokkaido University and written informed consent was obtained from all participants. Thirty-one patients with SSc, all of whom met the American College of Rheumatology preliminary criteria[16], were screened for our study. All patients developing SSc within the last 3 years onset fulfilled at least 1 of the following: early rapidly progressive diffuse skin sclerosis despite continuing treatment, refractory skin ulcers, interstitial lung disease confirmed by lung computed tomography (CT), reversible cardiac involvement such as arrhythmia and cardiomegaly, renal involvement with hypertension, persistent urinalysis abnormalities, and microangiopathic hemolytic anemia. Patients were excluded from the study when they were over 60 years old, or had uncontrolled arrhythmia, left ventricular ejection fraction on echocardiography below 45%, carbon dioxide diffusion lung capacity (DLCO) below 45% predicted, serum creatinine above 176.8 μmol/L (2.0 mg/dl) and glomerular filtration rate (GFR) below 40 ml/min/m^2. All enrolled patients were evaluated clinically at the time of diagnosis and on regular visits for followup.

Thirty-five healthy controls were also enrolled in the study.

Transplantation procedure and followup. The mobilization regimen comprised recombinant human granulocyte colony-stimulating factor (rhG-CSF) and intravenous cyclophosphamide (4 g/m^2). In 5 patients treated with CD34-HSCT, enriched CD34+ graft, prepared using CliniMACS® system (Miltenyi Biotec, Germany) was stored in liquid nitrate until use for transplant. Graft manipulation was not performed in the next 5 patients treated with unselected-HSCT.

We treated all SSc patients with intravenous cyclophosphamide (200 mg/kg, divided into 4 days) followed by autologous HSCT. rhG-CSF was administered from the second day of transplantation of frozen-thawed autologous enriched CD34+ grafts or frozen-thawed autologous unselected grafts. T cell depleting antibodies such as antithymocyte globulin, antilymphocyte globulin and anti-CD52 antibodies (Campath) were not administered in our patients.

We assessed the improvement of skin sclerosis by the modified Rodnan total thickness skin score (mRTSS). Electrocardiogram and echocardiography were used to evaluate the cardiac function, chest radiograph, chest high resolution CT, and spirometry to evaluate pulmonary function, renogram to evaluate renal function, and serological tests to assess other organ involvement and the presence of autoantibodies.

Lymphocyte phenotyping. Peripheral blood mononuclear cells (PBMC) were prepared from heparinized venous blood by Ficoll-Paque Plus® (Amersham Biosciences Corp., NJ, USA).

We assessed the subpopulation of peripheral lymphocytes by immunofluorescence staining of PBMC with anti-human CD3-Cy-Chrome, CD4-fluorescein isothiocyanate (FITC), CD8-FITC, CD19-FITC, TCRγδ-FITC, CD3-phycoerythrin (PE), CD8-PE, CD45RO-PE, CD25-PE, HLA-DR-PE, and CD69-PE (BD Biosciences Pharmingen, San Diego, CA).

The expression levels of interferon (IFN)-γ and interleukin (IL)-4 were studied in the cytoplasm of peripheral CD4+ or CD8+ T cells. Briefly, we stimulated PBMC with phorbol myristate acetate (50 ng/ml) and ionomycin (250 ng/ml) for 6 h in RPMI 1640 containing 10% heat-inactivated fetal bovine serum and monensin (2 μM) at 37°C in 5% carbon dioxide. We evaluated the IFN-γ or IL-4 expression on T cells by staining with anti-CD3-Cy-Chrome, anti-CD8-FITC and -PE, anti-IFN-γ-FITC, and anti-IL-4-PE using Cytofix/Cytoperm Plus® (BD Biosciences Pharmingen) according to the manufacturer's instructions. Immunostained cells were analyzed using a FACSCalibur™ flow cytometer (Becton Dickinson Immunocytometry Systems, San Jose, CA).

Quantification of thymic signal joint T cell receptor rearrangement excision circles (sjTREC). Thymic sjTREC on genomic DNA from PBMC was quantified by real-time quantitative polymerase chain reaction (PCR) (ABI PRISM® 7000; Applied Biosystems, Foster City, CA) according to the method of Douek, *et al*[17]. The sjTREC values were corrected by the percentage of CD3+ cells in the sample and were then expressed as numbers of sjTREC/μg of CD3+ cells DNA according to the method of Farge, *et al*[18]. Values were measured before autologous HSCT, then at 3, 6, and 12 months after autologous HSCT.

Quantification of foxp3 *gene expression levels.* Total RNA were isolated from PBMC using TRIzol® reagent (Invitrogen, Carlsbad, CA) according to the manufacturer's instructions. Total RNA (1 μg) was reverse transcribed by ReverTraAce (Toyobo, Osaka, Japan), in the presence of oligo(dT)12-18 primers (Invitrogen) according to the manufacturer's instructions. We performed real-time PCR using the ABI PRISM® 7000 Sequence Detection System and specific primers for *foxp3* and *gapdh* from TaqMan® Gene Expression Assays (Applied Biosystems).

Statistical analysis. We used the Mann-Whitney U-test to analyze the difference among each value otherwise indicated. The changes in mRTSS and phenotype of lymphocytes after the autologous HSCT were compared with values at inclusion using the Wilcoxon signed rank test. Female-male ratio in each group was assessed using Fisher's exact probability test. The sjTREC values in healthy individuals were assessed using the Spearman's correlation test. Calculations were performed using the statistical software package JMP version 5.0 (SAS Institute Inc., Cary, NC). P values less than 0.05 were considered significant.

RESULTS

Between November 2000 and July 2006, 11 consecutive patients meeting the criteria in our study were enrolled and 10 patients were transplanted out of 31 screened patients with SSc for autologous HSCT treatment. One patient was not transplanted because of her mobilization failure. First 5 patients were treated with CD34-HSCT. Subsequent 5 patients were treated with unselected-HSCT. The character-

Personal non-commercial use only. The Journal of Rheumatology Copyright © 2009. All rights reserved.

istics of patients treated with autologous HSCT are shown in Table 1. Mean age at inclusion, mean mRTSS before mobilization and mean durations from SSc onset to the treatment were similar between patients treated with CD34-HSCT and unselected-HSCT. Several treatments such as D-penicillamine, prostaglandin derivatives, and corticosteroids were not feasible for our patients. All patients were followed up until July 2007 (40.7 ± 25.6 mos).

Mean number of infused CD34+ cells was not different between CD34-HSCT and unselected-HSCT groups. Mean time needed to achieve a neutrophil count greater than 0.5 × 10^9/l and a platelet count greater than 50 × 10^9/l were not different between 2 groups. Cytomegalovirus antigenemia were shown in 3 patients out of all transplanted patients. Patient 2 had hemophagocytic syndrome on day 6. Patient 3 had adenoviral hemorrhagic cystitis on day 14 and engraftment syndrome on day 15. Patient 7 had engraftment syndrome on day 12. Hemophagocytic syndrome and engraftment syndrome responded to corticosteroid administration. Hemorrhagic cystitis was refractory to acyclovir, vidarabine, ganciclovir, or ribavirin. Patient 3 had the second autologous HSCT using unselected grafts at 3 months after first autologous HSCT using selected CD34+ cells due to recurrent infectious diseases.

Four out of 5 transplanted patients have more than a 25% fall in the skin score compared with baseline values in both groups (Figure 1). Dermal thickness assessed by skin biopsy was also improved in these patients with clinical benefits (data not shown). Additional unselected-HSCT at 3 months after CD34-HSCT did not affect Patient 3's skin manifestation. Cardiac and pulmonary functions were not altered significantly through the treatment in all patients (data not shown). Their serum level of γ-globulin almost remained normal range through autologous HSCT (data not shown). Their serum level of anti-Scl70 antibodies reduced except Patient 2 treated with CD34-HSCT (data not shown). Transplantation related complications during hospitalization are shown in Table 1. There was no significant difference in the incidence of adverse events between both groups and no transplantation related mortality.

We compared immunological reconstitution profile over time between good and poor response groups, and between CD34-HSCT and unselected-HSCT groups. First, we analyzed immunological reconstitution between good and poor response groups. Clinical response to therapy was categorized into major, partial, or no response, or disease progression or relapse according to the method of Farge, *et al*[13]. According to the observed clinical response compared to these criteria, 2 groups of patients were retrospectively constituted: good response group, consisting of 7 patients with sustained major or partial response, and poor response group, consisting of 3 patients (Patient 5, 6, and 7) with no

Table 1. Patients' profile at study inclusion and clinical findings at autologous hematopoietic stem cell transplantation (HSCT).

	Patients Treated with CD34-HSCT					Patients treated with Unselected-HSCT					Mean ± SD		
	1	2	3	4	5	6	7	8	9	10	CD34	Untreated	p
Age, yrs	57	19	54	48	52	43	19	42	30	28	46.0 ± 15.4	32.4 ± 10.1	0.094
Sex, female:male	M	F	F	F	M	M	F	F	F	F	3:2	4:1	1.000
mRTSS, 0–51	38	28	25	15	32	32	17	26	23	20	27.6 ± 8.6	23.6 ± 5.8	0.402
Disease duration, mo	21	31	21	12	36	16	24	18	8	12	24.2 ± 9.4	15.6 ± 6.1	0.141
Interstitial pneumonia	—	—	+	—	+	—	+	—	—	—	—	—	—
GFR, ml/min	76.53	121.43	101.43	114.39	99.32	139.29	120.3	101.8	82.62	103.42	102.6 ± 17.2	109.5 ± 21.3	0.465
DLCO %	83	66.8	52.2	90.9	83.8	92.5	54.7	113.4	48	94.4	75.3 ± 15.7	80.6 ± 28.0	0.465
γ-globulin, %	19.5	24.7	24.1	16.8	12.5	20.5	19.8	—	16.8	16.7	19.5 ± 5.1	18.5 ± 2.0	0.712
Anti-Scl 70, index	< 5	92.3	204.6	8.7	158.6	16.1	128.2	< 5	< 5	202	92.8 ± 90.2	69.3 ± 91.5	0.597
Prior therapies	PG	PG, D, PSL	PG, PSL	PG, PSL	D, PSL	PG	PG	D, PSL	D, PSL	PG	—	—	—
Mobilization	G	G + CYC	G + CYC	G + CYC	G + CYC	G + CYC	G + CYC	G + CYC	G + CYC	G + CYC	—	—	—
Conditioning	CYC	CYC	CYC	CYC	CYC	CYC	CYC	CYC	CYC	CYC	—	—	—
Infused CD34+ cells, × 10^6/kg	2.96	5.21	2.75	3.14	12.7	3.95	2.77	4.28	14.9	2.81	5.4 ± 4.2	5.7 ± 5.2	0.917
Purity, %	96	95	90	93.53	96.59	—	—	—	—	—	94.2 ± 2.6	—	—
Neutrophils > 0.5 × 10^9/l (day)	11	9	11	9	9	8	11	10	10	10	9.8 ± 1.1	9.8 ± 1.1	0.914
Platelets > 50 × 10^9/l (day)	15	21	16	8	11	0	8	11	11	12	14.2 ± 5.0	8.4 ± 4.9	0.138
Transplant related complications	CMV	CMV, HPS	CMV, HC, ES	—	—	—	ES	—	—	—	—	—	—

mRTSS: modified Rodnan total thickness skin score; PG: prostaglandin derivatives; D: d-penicillamine; PSL: prednisolone; G: granulocyte-colony-stimulating factor; CYC: cyclophosphamide; CMV: cytomegalovirus antigenemia; HPS: hemophagocytic syndrome; HC: hemorrhagic cystitis; ES: engraftment syndrome; GFR: glomerular filtration rate; DLCO: diffusion capacity for carbon monoxide.

Personal non-commercial use only. The Journal of Rheumatology Copyright © 2009. All rights reserved.

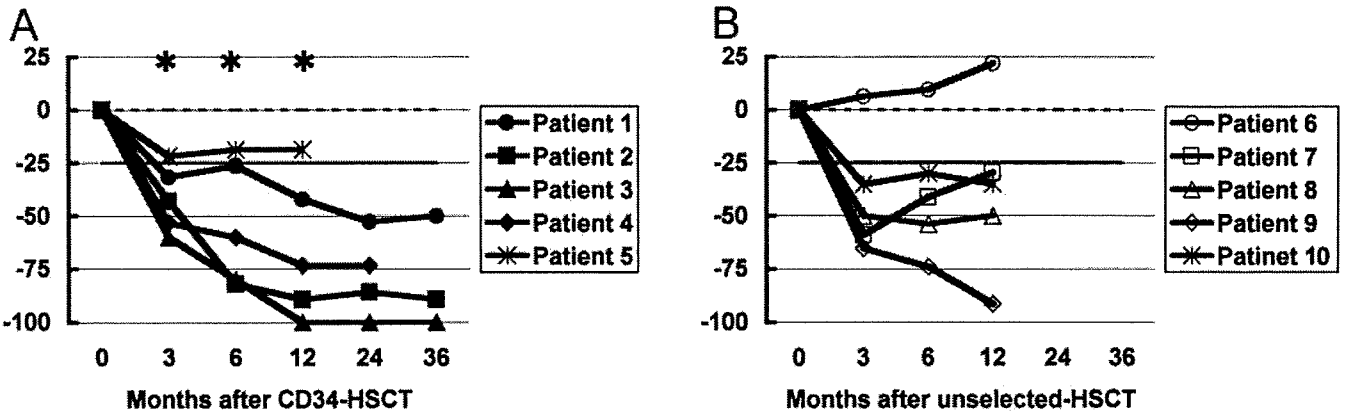

Figure 1. Evaluation of modified Rodnan total thickness skin score (mRTSS) in patients with systemic sclerosis. A. Changes of mRTSS in patients treated with CD34-HSCT. B. Changes of mRTSS in patients treated with unselected-HSCT. Proportional change from baseline measurement was calculated for each patient at each available timepoint. * $p < 0.05$.

response or with relapse of disease (Table 2). Our patients were evaluated by functional evaluation (performance status and/or health assessment questionnaire) and mRTSS with skin improvement assessed by skin biopsy. Each organ function was not altered significantly through the treatment in all patients. Mean age at inclusion, mean mRTSS before mobilization, and mean durations from onset scleroderma to treatment were similar between both groups. At inclusion, the ratio of CD4/CD8, the percentage of CD4+CD45RO+, CD4+CD45RO-, CD19+, CD4+CD25+, CD56+, CD3+TCRγδ+, IFN-γ- and IL-4-producing CD4+ and CD8+ cells were in the normal range for all patients and were not different between good and poor response groups (Table 3). After autologous HSCT, shortened CD4/CD8 ratio was sustained due to delayed CD4+ cell recovery and prompt CD8+ cell recovery in both groups. CD4+CD45RO-naive T cells remained low at 6 months after autologous HSCT in good response group, and CD4+CD45RO- cells reconstituted faster in poor response group ($p < 0.05$). CD19+ and CD56+ cells returned into the normal range at 3 months in both groups. The kinetics of other cells through autologous HSCT was not statistically different between good and poor response group in the study. To evaluate the T cell response against mitogen stimulation after autologous HSCT, mean fluorescence intensity of CD69 on CD3+ cells was investigated. CD69 expression levels on CD3+CD8+ and CD3+CD8- cells against mitogen were not different between healthy controls and patients with SSc before autologous HSCT, and its kinetics through autologous HSCT were similar in both groups (Table 3). Cytokine production in CD3+CD8- and CD3+CD8+ T cells was assessed by intracellular staining of IFN-γ and IL-4. Levels of cytokine production in CD3+CD8- and CD3+CD8+ cells were not different between both groups. IFN-γ producing CD8+ T cells increased after autologous HSCT in both groups (Table 3).

Thymic output assessed by sjTREC was analyzed to evaluate the mechanism of peripheral CD4+CD45RO- and CD4+CD25+ proliferation. In healthy controls, the sjTREC values negatively correlated with their age (Figure 2A, $p < 0.0001$, $r^2 = 0.44$). Nine out of 10 transplanted patients could be analyzed in the study. Their sjTREC values also negatively correlated with their age at inclusion of autologous HSCT (Figure 2B, $p = 0.002$, $r^2 = 0.80$). The sjTREC values were not significantly different between patients with SSc before autologous HSCT and age- and sex-matched

Table 2. Patients' profile between good and poor response groups at autologous HSCT.

	Good Response Group (n = 7)	Poor Response Group (n = 3)	p
Graft condition (CD34-HSCT: unselected)	4:3	1:2	1.000
Age, yrs	39.7 ± 14.4	38.0 + 17.1	0.819
Sex female: male	6:1	1:2	1.000
mRTSS (0–51)	25.0 ± 7.16	27.0 ± 8.66	0.568
Disease duration, mo	17.6 ± 7.72	25.3 ± 10.1	0.207
Infused CD34+ cells (× 10^6/kg)	5.15 ± 4.39	6.47 ± 5.42	0.909
Neutrophils > 0.5 × 10^9/l (day)	10.0 ± 0.82	9.33 ± 1.53	0.407
Platelets > 50 × 10^9/l (day)	13.4 ± 4.28	6.33 ± 5.69	0.064

mRTSS: modified Rodnan total thickness skin score.

Personal non-commercial use only. The Journal of Rheumatology Copyright © 2009. All rights reserved.

Table 3. Phenotype analysis of lymphocyte population through autologous HSCT between patients with good and poor clinical response. Value are mean ± SD.

	Normal Range 95% CI	At Inclusion		3 mo After HSCT		6 mo After HSCT		12 mo After HSCT	
		Good	Poor	Good	Poor	Good	Poor	Good	Poor
CD3+, CD4+	57.57–68.89	48.16 ± 18.77	52.34 ± 6.56	20.84 ± 9.75*	34.42 ± 7.66	23.18 ± 15.00*	45.23 ± 10.74	27.65 ± 15.61***	43.07 ± 9.72
CD3+, CD8+	26.47–37.68	25.91 ± 9.32	33.92 ± 13.66	48.07 ± 21.57	49.64 ± 11.44	35.78 ± 15.44	49.69 ± 13.09	44.97 ± 13.94	47.56 ± 10.43
CD4/CD8	0.61–2.96 (ratio)	2.11 ± 1.31	1.74 ± 0.72	0.43 ± 0.13*	0.71 ± 0.15	0.66 ± 0.35*	1.01 ± 0.56	0.61 ± 0.28	0.96 ± 0.39
CD3+, TCRγδ+	0.74–9.48	3.03 ± 3.05	2.03 ± 1.19	5.11 ± 4.49	2.34 ± 0.84	2.75 ± 1.48	3.02 ± 1.86	4.18 ± 2.72	2.71 ± 1.80
CD4+, CD45RO–	5.23–42.08	28.51 ± 10.29	31.36 ± 8.40	3.43 ± 2.49*	7.89 ± 5.21	4.66 ± 2.93*	10.01 ± 8.46	7.12 ± 5.18	12.55 ± 10.78
CD4+, CD45RO+	9.00–27.97	17.08 ± 5.53	15.35 ± 3.87	15.48 ± 6.23	19.34 ± 5.87	13.68 ± 7.31	16.42 ± 4.85	14.32 ± 4.08	13.89 ± 4.10
CD4+, HLA-DR+	0.92–3.38	2.38 ± 0.86	3.95 ± 2.10	8.51 ± 4.99	12.58 ± 3.23	5.77 ± 4.58	7.12 ± 0.50	5.36 ± 4.16	5.20 ± 2.46
CD4+, CD25+	1.35–5.46	4.12 ± 3.36	5.45 ± 2.79	3.42 ± 2.21	6.12 ± 5.51	3.43 ± 2.67	7.54 ± 3.36	3.55 ± 2.28	4.62 ± 3.92
foxp3 mRNA	32.01–393.07 (copies/GAPDH 1 k copies)	563.39 ± 704.09	259.60 ± 247.27	182.74 ± 150.35	99.31 ± 29.61	201.77 ± 114.85	212.28 ± 121.62	214.00 ± 109.77	166.29 ± 133
CD3+, CD8–, IFNγ+	0.67 ± 17.49	6.05 ± 6.55	2.73 ± 0.60	12.16 ± 10.07	7.06 ± 5.20	8.21 ± 5.36	11.47 ± 8.02	9.29 ± 4.17	4.23 ± 3.66
CD3+, CD8–, IL4+	0.02–2.47	1.09 ± 0.55	1.39 ± 1.30	3.74 ± 2.63	2.50 ± 1.04	2.40 ± 2.13	4.96 ± 6.27	1.57 ± 1.24	1.20 ± 0.58
Th1/Th2	3.79–125.60 (ratio)	17.38 ± 21.04	4.98 ± 3.77	32.47 ± 52.40	107.75 ± 154.29	32.09 ± 45.55	67.05 ± 59.15	24.82 ± 23.42	23.75 ± 36.56
CD3+, CD8+, IFNγ+	0.66–41.60	5.73 ± 6.15	5.25 ± 3.11	29.83 ± 21.39*	19.80 ± 11.29	17.43 ± 13.55	25.93 ± 13.92	27.71 ± 19.13	3.29 ± 4.95
CD3+, CD8+, IL4+	0.00–1.40	0.19 ± 0.17	0.25 ± 0.38	0.86 ± 0.79	0.54 ± 0.38	1.01 ± 1.24	0.68 ± 0.68	0.72 ± 0.45	0.16 ± 0.15
Tc1/Tc2	7.83–185.08 (ratio)	89.68 ± 98.17	56.15 ± 71.29	154.35 ± 217.62	1492.65 ± 2280.82	88.36 ± 78.79	1460.06 ± 1262.52	80.27 ± 76.12	41.91 ± 71.92
CD3+, CD8–, CD69+	82.91–201.89 (MFI)	177.55 ± 90.61	121.10 ± 84.95	58.25 ± 41.65	28.34 ± 12.87	63.06 ± 37.00	67.76 ± 40.69	89.54 ± 42.85	38.52 ± 33.83
CD3+, CD8+, CD69+	54.27–119.07 (MFI)	106.82 ± 35.27	96.05 ± 64.04	30.92 ± 20.39	24.94 ± 12.97	31.00 ± 19.98	53.89 ± 30.39	61.82 ± 19.69	30.83 ± 19.29
CD19+	5.00–32.98	16.16 ± 7.54	12.69 ± 9.40	21.91 ± 22.58	14.40 ± 7.64	27.01 ± 22.93	9.50 ± 5.73	18.60 ± 10.83	11.13 ± 3.99
CD56+	8.94–22.94	13.17 ± 11.67	11.83 ± 7.68	14.11 ± 6.97	9.93 ± 4.49	8.99 ± 2.96	19.83 ± 11.87	12.05 ± 7.58	14.12 ± 7.61

* The value from the baseline measurement was calculated for each value at each timepoint. $p < 0.05$. MFI: mean fluorescence intensity.

healthy controls ($p = 0.8253$). The sjTREC values were significantly suppressed at 3 months after autologous HSCT in the good response group compared with poor responders (Figure 2C, $p = 0.0152$), although the values were not different at inclusion, 6 and 12 months after autologous HSCT between both groups.

Foxp3 is a key regulatory gene for the development of regulatory T cells[19]. *Foxp3* gene expressions in PBMC were analyzed to assess the relationship between the recovery of CD4+CD25+ cells including regulatory T cells and clinical benefits in transplanted SSc patients. *Foxp3* gene expressions in PBMC were within the normal range through autologous HSCT and were not different in the 2 groups (Table 3).

Next, immunological reconstitution was analyzed between CD34-HSCT and unselected-HSCT groups to assess how graft manipulation affected immune system and clinical response. At inclusion, the ratio of CD4/CD8, the percentage of CD4+CD45RO-, CD4+CD45RO+, CD19+, CD4+CD25+, CD56+, CD3+TCRγδ+, IFN-γ, and IL-4 producing CD4+ and CD8+ cells were in the normal range for all patients and did not differ between CD34-HSCT and unselected-HSCT. After autologous HSCT, CD4/CD8 ratio remained low in both groups. In CD4+ subsets, CD4+CD45RO-, CD4+HLA-DR+, and CD4+CD25+ cells increased rapidly in unselected-HSCT compared with CD34-HSCT at 12 months ($p < 0.05$, Table 4). CD19+ and CD56+ cells returned into the normal range at 3 months in both groups. CD69 expression levels on CD3+CD8+ and CD3+CD8- cells against mitogen were not different between healthy controls and patients with SSc before autologous HSCT, and its kinetics through autologous HSCT were similar in both groups (Table 4). Levels of cytokine production in CD3+CD8- and CD3+CD8+ cells were not different between both groups. IFN-γ-producing CD3+CD8+ T cells increased after autologous HSCT in both groups (Table 4).

Cytokine production in CD8- and CD8+ T cells was assessed by intracellular IFN-γ and IL-4. Cytokine production in CD8- cells was not different between both groups. IFN-γ- and IL-4-producing CD8+ T cells increased after autologous HSCT in both groups (Table 4).

The sjTREC values recovered to the levels at inclusion between 6 to 12 months after CD34-HSCT or unselected-HSCT. There was no statistical significance through their clinical course in both groups (Figure 2D).

Foxp3 gene expressions in PBMC were within the normal range through autologous HSCT and not different in the 2 groups (Table 4).

Personal non-commercial use only. The Journal of Rheumatology Copyright © 2009. All rights reserved.

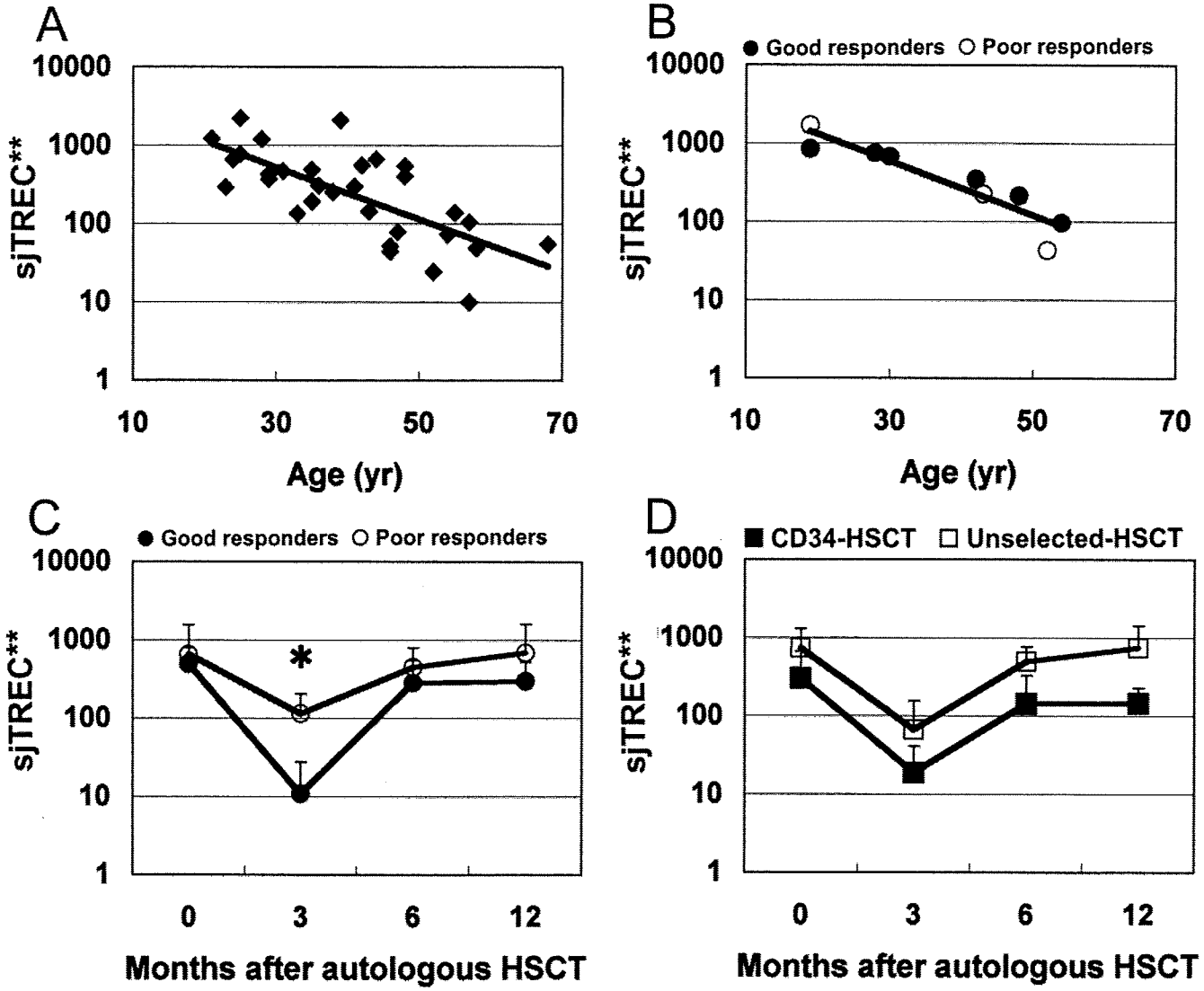

Figure 2. sjTREC values in CD3+ cells in healthy individuals and its kinetics through autologous HSCT. A. Relation between age and numbers of sjTRECs in healthy controls. B. Relation between age and numbers of sjTREC in SSc patients treated with autologous HSCT. C. sjTREC between good and poor response groups. D. sjTREC between patients treated with CD34-HSCT and unselected-HSCT. Logarithmic scales were used for y-axes to compress the figure. * p = 0.0152. **copies/μg in CD3+ cells DNA.

DISCUSSION

We described the efficacy and the safety in patients with SSc treated with autologous HSCT. More than a 25% decrease in the skin score, which correlates with patient's survival[20], was achieved in 8 out of 10 transplanted SSc patients. Skin improvement was not significantly different between CD34-HSCT and unselected-HSCT groups. In addition, additional unselected-HSCT did not lead to recurrence or adverse effect on skin manifestation in Patient 3. These results suggest that graft condition did not affect the clinical outcome on skin involvement up to 12 months after autologous HSCT in our series.

Few data on thymic function and lymphocyte phenotypes after autologous HSCT have been reported in transplanted SSc patients[13,18,21]. The TREC values might be related to clinical response in our transplanted patients. In the last decade, basic and clinical scientists have focused a role of sjTREC as a marker of human thymic function[22]. Values of sjTREC can also reflect the pathophysiology in patients with autoimmune diseases. The sjTREC values may be affected by disease activity in patients with systemic lupus erythematosus[23]. Age-inappropriate T cell senescence confirmed by decreased frequency of sjTREC may also contribute to the development of juvenile idiopathic arthritis[24]. There was no evidence to prove an age-inappropriate T cell senescence and a correlation between the sjTREC values

Personal non-commercial use only. The Journal of Rheumatology Copyright © 2009. All rights reserved.

Table 4. Phenotype analysis of lymphocyte population through autologous HSCT between patients with CD34-HSCT and unselected-HSCT. Values are mean ± SD.

	Normal Range 95% CI	At Inclusion CD34–HSCT	At Inclusion un-HSCT	3 mo After HSCT CD34-HSCT	3 mo After HSCT un-HSCT	6 mo After HSCT CD34-HSCT	6 mo After HSCT un-HSCT	12 mo After HSCT CD34-HSCT	12 mo After HSCT un-HSCT
CD3+, CD4+	57.57–68.89	37.84 ± 11.45	60.99 ± 9.66	17.85 ± 9.95	31.98 ± 6.69*	20.30 ± 14.73	43.31 ± 9.75	24.13 ± 14.36*	43.62 ± 8.46
CD3+, CD8+	26.47–37.68	22.20 ± 6.45	34.42 ± 11.06	36.07 ± 18.09	61.02 ± 6.96	33.69 ± 15.89	48.83 ± 11.58	42.02 ± 14.06	50.60 ± 9.08
CD4/CD8	0.61–2.96 (ratio)	1.87 ± 0.87	2.13 ± 1.45	0.49 ± 0.22*	0.54 ± 0.18*	0.62 ± 0.36*	0.97 ± 0.48	0.58 ± 0.28*	0.91 ± 0.35
CD3+, TCRγδ+	0.74–9.48	3.66 ± 3.44	1.80 ± 1.09	4.31 ± 5.13	4.24 ± 2.90	2.54 ± 1.62	3.21 ± 1.48	4.03 ± 2.78	2.85 ± 1.52
CD4+, CD45RO–	5.23–42.08	29.10 ± 7.34	29.63 ± 12.01	4.58 ± 5.44*	4.95 ± 1.91*	4.94 ± 3.36*	8.33 ± 7.59	4.29 ± 2.23*	14.73 ± 7.39
CD4+, CD45RO+	9.00–27.97	15.56 ± 4.16	17.57 ± 5.93	13.79 ± 6.90	19.48 ± 3.92	14.20 ± 7.61	15.09 ± 5.65	13.02 ± 3.83	16.32 ± 2.91
CD4+, HLA-DR+	0.92–3.38	2.90 ± 1.36	2.80 ± 1.66	7.61 ± 5.72	11.85 ± 2.72	4.36 ± 2.32	8.54 ± 4.03	2.92 ± 0.56	8.29 ± 3.34
CD4+, CD25+	1.35–5.46	2.70 ± 1.67	6.33 ± 3.28	2.30 ± 1.10	5.94 ± 4.07	3.33 ± 3.20	6.64 ± 2.98	2.02 ± 0.95	6.27 ± 2.24
foxp3 mRNA	32.01–393.07 (copies/GAPDH 1k copies)	524.44 ± 880.90	420.07 ± 199.61	110.72 ± 100.54	204.72 ± 149.57	129.22 ± 101.19	280.62 ± 51.70	123.34 ± 60.37	291.54 ± 87.8
CD3+, CD8–, IFNγ+	0.67–17.49	6.65 ± 8.28	3.58 ± 1.62	13.59 ± 10.75	7.95 ± 6.99	9.60 ± 4.19	9.27 ± 8.38	5.64 ± 3.27	17.44 ± 10.45
CD3+, CD8–, IL4+	0.02–2.47	0.85 ± 0.59	1.46 ± 0.89	4.51 ± 2.41	2.38 ± 1.75	2.98 ± 1.95	3.74 ± 5.68	1.97 ± 0.90	0.61 ± 0.31
Th1/Th2	3.79–125.60 (ratio)	20.41 ± 26.40	7.51 ± 4.67	13.88 ± 15.28	96.22 ± 120.52	31.49 ± 37.45	68.90 ± 75.09	13.81 ± 23.54	37.78 ± 25.33
CD3+, CD8+, IFNγ+	0.66–41.60	8.31 ± 6.99	3.38 ± 1.47	27.35 ± 22.64	25.80 ± 17.33	30.29 ± 10.03	10.94 ± 8.31	24.77 ± 25.94	12.34 ± 10.07
CD3+, CD8+, IL4+	0.00–1.40	0.23 ± 0.21	0.20 ± 0.28	1.11 ± 0.83	0.46 ± 0.40	1.26 ± 1.27	0.51 ± 0.65	0.81 ± 0.47	0.22 ± 0.17
Tc1/Tc2	7.83–185.08 (ratio)	49.51 ± 62.39	101.70 ± 103.52	127.14 ± 120.21	984.54 ± 1771.58	550.91 ± 974.27	654.58 ± 1136.02	60.02 ± 89.13	76.82 ± 57.32
CD3+, CD8–, CD69+	82.91–201.89 (MFI)	172.45 ± 122.20	147.75 ± 62.66	59.53 ± 53.14	39.28 ± 18.77	68.95 ± 37.16	57.96 ± 39.23	84.12 ± 47.34	47.57 ± 39.01
CD3+, CD8+, CD69+	54.27–119.07 (MFI)	82.70 ± 45.77	119.66 ± 36.51	18.72 ± 5.52	37.09 ± 20.28	33.35 ± 25.06	49.98 ± 26.42	50.73 ± 14.13	49.30 ± 40.58
CD19+	5.00–32.98	18.20 ± 8.43	12.04 ± 6.42	21.84 ± 28.33	17.47 ± 3.07	24.44 ± 24.80	14.05 ± 4.86	18.12 ± 10.94	13.93 ± 5.86
CD56+	8.94–22.94	13.42 ± 13.69	12.12 ± 6.82	12.67 ± 6.43	13.05 ± 7.12	13.79 ± 11.12	11.11 ± 4.10	14.65 ± 7.56	9.74 ± 5.19

* The value from the baseline measurement was calculated for each value at each timepoint. $p < 0.05$. MFI: mean fluorescence intensity.

and disease condition in our patients with SSc. Thymic function assessed by sjTREC values is significantly suppressed at engraftment, recovers within 3 months after autologous HSCT, and is age-dependent in adults[17,25]. In our series, the lower level of sjTREC at 3 months after autologous HSCT was shown in the good response group without dependence on their age and graft condition. Longterm defects of CD3+CD4+ cells, especially CD4+CD45RO-naïve T cells, after autologous HSCT might also reflect profound suppression of thymopoiesis in the good response group. Thymus-dependent immunological reconstitution leads to the T cell precursor reeducation and renewal of the T cell repertoire, and may induce remission of autoimmunity[26,27]. Our results suggest that transient, profound suppression of thymic function might alter immune condition, leading to clinical response in patients with SSc.

Peripheral immunological reconstitution after autologous CD34-HSCT or unselected-HSCT has been well documented in patients with hematological disorders[28-30]. While CD56+ cells, followed by CD19+ cells, recover promptly after autologous HSCT, CD3+ cells, especially CD4+CD45RO- cells, remain low after autologous HSCT in CD34-HSCT and unselected-HSCT[29,30]. After the initial 2 months of autologous HSCT, IFN-γ-producing CD8+ or CD8- T cells remain normal or increased[11,30]. In our series, kinetics of lymphocytes recovery is similar to these previous results. In patients with SSc, peripheral blood T cells show a predominantly type 2 T-helper profile, and can induce fibrosis through the production of cytokines, especially IL-4[2]. Cytokine production in T cells at inclusion was not significantly different between our transplanted patients with SSc and healthy controls. The kinetics of IFN-γ- and IL-4-producing T cells after autologous HSCT was not different between CD34-HSCT and unselected-HSCT, or good and poor response groups. Therefore, the significance of cytokine production in T cells after autologous HSCT was not conclusive. In good response group with sustained major or partial response, phenotype or function of peripheral lymphocytes was not significantly different from that of poor response group through autologous HSCT. These results suggest that changes in peripheral immunity were not correlated with clinical response.

CD4+CD25+FOXP3+ regulatory T cells may play a role in the immunological reconstitution leading to the improvement of autoimmune disease or prevention of graft-versus-host disease after autologous or allogeneic HSCT[31,32]. Although CD4+CD25+ population increased at 12 months after autologous HSCT in unselected-HSCT compared with

Personal non-commercial use only. The Journal of Rheumatology Copyright © 2009. All rights reserved.

that in CD34-HSCT, it is noted that there was no difference between good and poor response groups, and *foxp3* gene expression levels did not correlate with the clinical response or with graft condition. CD4+CD25+ populations include non-regulatory activated T cells as well as regulatory T cells[32]. Increased CD4+CD25+ population might reflect the activation of CD4+ T cells because CD4+HLA-DR+ population also increased at 12 months in unselected-HSCT group. Therefore, the role of CD4+CD25+ regulatory T cells on clinical response was not evident in our study.

Although the importance of graft manipulation in autologous HSCT for autoimmune diseases has been debated, clinical outcome may not necessarily correlate with the autoreactive clone survival after CD34-HSCT[33]. In patients with rheumatoid arthritis, a pilot study showed that clinical response and laboratory findings were also similar between CD34-HSCT and unselected-HSCT[12]. In addition, autoimmunity after autologous HSCT may result from the type of conditioning regimen rather than graft condition (i.e., CD34-HSCT or unselected-HSCT)[34]. Although peripheral immunity after autologous HSCT does not have a decisive impact on disease control in our transplanted SSc patients, further study will reveal the role of peripheral immunity after autologous HSCT. Our results suggest the relationship between clinical benefits and immunosuppression intensity sufficient to suppress thymic output by the treatment.

The results of our study suggest that immunosuppression sufficient to downregulate thymic function, rather than the graft manipulation, can lead to clinical benefits in patients with SSc. Additionally, appropriately monitoring the sjTREC values after autologous HSCT may serve to identify patients who would not achieve clinical remission by autologous HSCT and additional treatment in a more timely way.

ACKNOWLEDGMENT

We thank Drs. Masaya Mukai (Sapporo City General Hospital), Satoshi Jodo (Tomakomai City Hospital), Katsunori Onishi (Sapporo Social Insurance General Hospital), Hideki Kasahara (NTT East Corporation Sapporo Hospital), and Noriyuki Sakurai (Minami Sapporo Hospital) for clinical procedures.

REFERENCES

1. Charles C, Clements P, Furst DE. Systemic sclerosis: hypothesis-driven treatment strategies. Lancet 2006;367:1683-91.
2. Sakkas LI, Chikanza IC, Platsoucas CD. Mechanisms of Disease: the role of immune cells in the pathogenesis of systemic sclerosis. Nat Clin Pract Rheumatol 2006;2:679-85.
3. Varga J, Abraham D. Systemic sclerosis: a prototypic multisystem fibrotic disorder. J Clin Invest 2007;117:557-67.
4. Alaez C, Loyola M, Murguia A, et al. Hematopoietic stem cell transplantation (HSCT): an approach to autoimmunity. Autoimmun Rev 2006;5:167-79.
5. Sykes M, Nikolic B. Treatment of severe autoimmune disease by stem-cell transplantation. Nature 2005;435:620-7.
6. Passweg J, Tyndall A. Autologous stem cell transplantation in autoimmune diseases. Semin Hematol 2007;44:278-85.
7. Vonk MC, Marjanovic Z, van den Hoogen FH, et al. Long-term follow-up results after autologous haematopoietic stem cell transplantation for severe systemic sclerosis. Ann Rheum Dis 2008;67:98-104.
8. Nash RA, McSweeney PA, Crofford LJ, et al. High-dose immunosuppressive therapy and autologous hematopoietic cell transplantation for severe systemic sclerosis: long-term follow-up of the US multicenter pilot study. Blood 2007;110:1388-96.
9. Farge D, Passweg J, van Laar JM, et al. Autologous stem cell transplantation in the treatment of systemic sclerosis: report from the EBMT/EULAR Registry. Ann Rheum Dis 2004;63:974-81.
10. de Buys P, Khanna D, Furst DE. Hemopoietic stem cell transplantation in rheumatic diseases—an update. Autoimmun Rev 2005;4:442-9.
11. Endo T, Sato N, Koizumi K, et al. A preliminary analysis of the balance between Th1 and Th2 cells after CD34+ cell-selected autologous PBSC transplantation. Cytotherapy 2004;6:337-43.
12. Moore J, Brooks P, Milliken S, et al. A pilot randomized trial comparing CD34-selected versus unmanipulated hemopoietic stem cell transplantation for severe, refractory rheumatoid arthritis. Arthritis Rheum 2002;46:2301-9.
13. Farge D, Marolleau JP, Zohar S, et al. Autologous bone marrow transplantation in the treatment of refractory systemic sclerosis: early results from a French multicentre phase I-II study. Br J Haematol 2002;119:726-39.
14. Traynor AE, Schroeder J, Rosa RM, et al. Treatment of severe systemic lupus erythematosus with high-dose chemotherapy and haemopoietic stem-cell transplantation: a phase I study. Lancet 2000;356:701-7.
15. Muraro PA, Douek DC, Packer A, et al. Thymic output generates a new and diverse TCR repertoire after autologous stem cell transplantation in multiple sclerosis patients. J Exp Med 2005;20:805-16.
16. Preliminary criteria for the classification of systemic sclerosis (scleroderma). Subcommittee for scleroderma criteria of the American Rheumatism Association Diagnostic and Therapeutic Criteria Committee. Arthritis Rheum 1980;23:581-90.
17. Douek DC, Vescio RA, Betts MR, et al. Assessment of thymic output in adults after haematopoietic stem-cell transplantation and prediction of T-cell reconstitution. Lancet 2000;355:1875-81.
18. Farge D, Henegar C, Carmagnat M, et al. Analysis of immune reconstitution after autologous bone marrow transplantation in systemic sclerosis. Arthritis Rheum 2005;52:1555-63.
19. Hori S, Nomura T, Sakaguchi S. Control of regulatory T cell development by the transcription factor Foxp3. Science 2003;299:1057-61.
20. Steen VD, Medsger TA, Jr. Improvement in skin thickening in systemic sclerosis associated with improved survival. Arthritis Rheum 2001;44:2828-35.
21. McSweeney PA, Nash RA, Sullivan KM, et al. High-dose immunosuppressive therapy for severe systemic sclerosis: initial outcomes. Blood 2002;100:1602-10.
22. Douek DC, McFarland RD, Keiser PH, et al. Changes in thymic function with age and during the treatment of HIV infection. Nature 1998;396:690-5.
23. Vieira QF, Kayser C, Kallas EG, Andrade LE. Decreased recent thymus emigrant number is associated with disease activity in systemic lupus erythematosus. J Rheumatol 2008;35:1762-7.
24. Prelog M, Schwarzenbrunner N, Sailer-Hock M, et al. Premature aging of the immune system in children with juvenile idiopathic arthritis. Arthritis Rheum 2008;58:2153-62.
25. Hakim FT, Memon SA, Cepeda R, et al. Age-dependent incidence, time course, and consequences of thymic renewal in adults. J Clin Invest 2005;115:930-9.
26. Williams KM, Hakim FT, Gress RE. T cell immune reconstitution

Personal non-commercial use only. The Journal of Rheumatology Copyright © 2009. All rights reserved.

following lymphodepletion. Semin Immunol 2007;19:318-30.
27. Muraro PA, Douek DC. Renewing the T cell repertoire to arrest autoimmune aggression. Trends Immunol 2006;27:61-7.
28. Guillaume T, Rubinstein DB, Symann M. Immune reconstitution and immunotherapy after autologous hematopoietic stem cell transplantation. Blood 1998;92:1471-90.
29. Damiani D, Stocchi R, Masolini P, et al. CD34+-selected versus unmanipulated autologous stem cell transplantation in multiple myeloma: impact on dendritic and immune recovery and on complications due to infection. Ann Oncol 2003;14:475-80.
30. Te Boekhorst PA, Lamers CH, Schipperus MR, et al. T-lymphocyte reconstitution following rigorously T-cell-depleted versus unmodified autologous stem cell transplants. Bone Marrow Transplant 2006;37:763-72.
31. de Kleer I, Vastert B, Klein M, et al. Autologous stem cell transplantation for autoimmunity induces immunologic self-tolerance by reprogramming autoreactive T cells and restoring the CD4+CD25+ immune regulatory network. Blood 2006;107:1696-702.
32. Roncarolo MG, Battaglia M. Regulatory T-cell immunotherapy for tolerance to self antigens and alloantigens in humans. Nat Rev Immunol 2007;7:585-98.
33. Bohgaki T, Atsumi T, Koike T. Multiple Autoimmune Diseases after Autologous Stem-Cell Transplantation. N Engl J Med 2007;357:2734-6.
34. Loh Y, Oyama Y, Statkute L, et al. Development of a secondary autoimmune disorder after hematopoietic stem cell transplantation for autoimmune diseases: role of conditioning regimen used. Blood 2007;109:2643-548.

Personal non-commercial use only. The Journal of Rheumatology Copyright © 2009. All rights reserved.

The American Journal of Pathology, Vol. 174, No. 1, January 2009
Copyright © American Society for Investigative Pathology
DOI: 10.2353/ajpath.2009.080573

Epithelial and Mesenchymal Cell Biology

Type XVII Collagen is a Key Player in Tooth Enamel Formation

Takuya Asaka,*† Masashi Akiyama,* Takanori Domon,‡ Wataru Nishie,* Ken Natsuga,* Yasuyuki Fujita,* Riichiro Abe,* Yoshimasa Kitagawa,† and Hiroshi Shimizu*

From the Department of Dermatology, Hokkaido University Graduate School of Medicine, Sapporo; Oral Diagnosis and Oral Medicine,† the Department of Oral Pathobiological Science, and the Division of Oral Functional Science,‡ the Department of Oral Functional Anatomy, Hokkaido University Graduate School of Dental Medicine, Sapporo, Japan*

Inherited tooth enamel hypoplasia occurs due to mutations in genes that encode major enamel components. Enamel hypoplasia also has been reported in junctional epidermolysis bullosa, caused by mutations in the genes that encode type XVII collagen (COL17), a component of the epithelial-mesenchymal junction. To elucidate the pathological mechanisms of the enamel hypoplasia that arise from the deficiency of epithelial-mesenchymal junction molecules, such as COL17, we investigated tooth formation in our recently established *Col17*$^{-/-}$ and *Col17* rescued mice. Compared with wild-type mice, the incisors of the *Col17*$^{-/-}$ mice exhibited reduced yellow pigmentation, diminished iron deposition, delayed calcification, and markedly irregular enamel prisms, indicating the presence of enamel hypoplasia. The molars of the *Col17*$^{-/-}$ mice demonstrated advanced occlusal wear. These abnormalities were corrected in the *Col17* rescued humanized mice. Thus, the *Col17*$^{-/-}$ mice clearly reproduced the enamel hypoplasia in human patients with junctional epidermolysis bullosa. We were able to investigate tooth formation in the *Col17*$^{-/-}$ mice because the *Col17*$^{-/-}$ genotype is not lethal. *Col17*$^{-/-}$ mouse incisors had poorly differentiated ameloblasts that lacked enamel protein-secreting Tomes' processes and reduced mRNA expression of amelogenin, ameloblastin, and of other enamel genes. These findings indicated that COL17 regulates ameloblast differentiation and is essential for normal formation of Tomes' processes. In conclusion, COL17 deficiency disrupts the epithelial-mesenchymal interactions, leading to both defective ameloblast differentiation and enamel malformation. ***(Am J Pathol 2009, 174:91–100; DOI: 10.2353/ajpath.2009.080573)***

Mesenchymal-epithelial interactions are thought to play essential roles in development of epithelial organs including the epidermis, hair follicles, and teeth. A variety of soluble factors, cell surface markers, and signal molecules have been reported to be involved in mesenchymal-epithelial interactions.[1,2] The hemidesmosome is a subcellular junctional adhesion structure overlying the basement membrane between the mesenchyme and epithelial cells that binds the epithelial cells to the underlying mesenchymal tissue.[3] Type XVII collagen (COL17) previously called "bullous pemphigoid antigen 2" or "BP180," is a transmembrane glycoprotein expressed in stratified and complex epithelia, such as the skin, the mucous membrane, and the eye, where it plays a crucial role in hemidesmosome stability and epithelial-mesenchymal attachment.[4]

Non-Herlitz junctional epidermolysis bullosa (nH-JEB) caused by COL17 deficiency shows the abnormal tooth formation of amelogenesis imperfecta.[5–7] We therefore hypothesized that COL17 in hemidesmosomes also plays an important role in mesenchymal-epithelial interactions in tooth formation.

Enamel formation is easily disrupted and enamel defects may reflect more than just genetic abnormalities. Enamel defects can also be attributed to environmental factors that cause chronological hypoplasia of the enamel during the enamel formation period.[7] It is important to study the pathomechanisms of enamel malformation in mice with defects in hemidesmosome components. There are several model mice with epithelial mesenchymal junction (EMJ) component deficiencies.[3,8] Among them, only laminin332-deficient mice are expected to have tooth malformation. However, the laminin332 knockout mice are

Supported in part by Grant-in-Aid from the Ministry of Education, Science, Sports and Culture of Japan to M. Akiyama (Kiban 20390304).

Accepted for publication September 30, 2008.

Address reprint requests to Masashi Akiyama, M.D., Ph.D., Department of Dermatology, Hokkaido University Graduate School of Medicine, North 15 West 7, Kita-ku, Sapporo 060-8638, Japan. E-mail: akiyama@med.hokudai.ac.jp.

lethal in their early development and tooth abnormality in adult mice has not been examined sufficiently.[8]

The *Col17* knockout (*Col17*$^{-/-}$) mice that we established recently are not lethal at birth; thus, we can use them to investigate the pathomechanisms of enamel defects that arise from hemidesmosome component deficiency.

To clarify the roles of COL17 in tooth formation, we studied the detailed process of tooth formation in *Col17* knockout (*Col17*$^{-/-}$) mice, which we recently established.[9] We show that COL17 has a critical role in tooth formation, especially in the differentiation of ameloblasts and enamelization, suggesting the importance of junction structure in mesenchymal-epithelial interaction during tooth formation.

Materials and Methods

Generation of *Col17*$^{-/-}$ Mice and Rescued COL17-Humanized Mice

The procedure for generating COL17$^{-/-}$ mice has been described.[9] Briefly, we cloned a 14.7-kb mouse genomic DNA COL17 fragment from the mouse 129Sv/Ev genomic library (Stratagene, La Jolla, CA). We subcloned a 11.5-kb *Nhe*I to *Not*I fragment to make the targeting vector. We inserted the PGK/Neo cassette between 6-bp upstream of the ATG start codon in exon 2 and 1.2-kb downstream in intron 2. We transfected the targeting vector by electroporation into 129 Sv/Ev embryonic stem cells, then microinjected the correctly targeted embryonic stem cell line into blastocysts obtained from C57BL/6J mice (Jackson Laboratory, Bar Harbor, Maine) to generate chimeric mice, which we then mated with C57BL/6J females. We crossed F1 heterozygotes with C57BL/6J for more than four generations and then intercrossed them to generate *Col17*$^{-/-}$ mice. The procedures for screening *Col17*$^{-/-}$ mice by PCR, reverse transcription (RT)-PCR, Northern and Western blotting, histology, electron microscopy, and immunofluorescence are described elsewhere.[9]

The phenotypic features of the *Col17* knockout (*Col17*$^{-/-}$) mice closely resembled those seen in nH-JEB (OMIM: 226650) caused by null mutations in the *COL17A1* gene, as previously described.[9] The *Col17*$^{-/-}$ mice had skin blisters and erosions from mild trauma. *Col17*$^{-/-}$ mice skin showed subepidermal blistering associated with a lack of COL17 and poorly formed hemidesmosomes.

Procedures for generating COL17-rescued mice have been described elsewhere.[9] Briefly, we crossed transgenic mice (C57BL/6 background) expressing the squamous epithelium-specific K14 promoter and a human *COL17* cDNA (*Col17*$^{m+/+}$, *COL17*$^{h+}$) with heterozygous *Col17*$^{m+/-}$ mice. Mice that carried both the heterozygous null mutation of *Col17* and the transgene of human *Col17* (*Col17*$^{m+/-}$, *COL17*$^{h+}$) were bred to produce rescued *Col17*$^{m-/-}$, *COL17*$^{h+}$ COL17-humanized mice.

The rescued mice showed almost none of the abnormal manifestations seen in the *Col17*$^{-/-}$ mice.[9]

Structural Analysis of Mouse Dentition

Tissue samples of mice were incubated in hot (approximately 90°C) distilled water for several minutes, and soaked in 10% Tasinase (Kyowa-hakkou, Tokyo, Japan) at 37°C for 6 hours. Incisors and first molars were taken from maxillomandibular tissue by removal of soft tissue. The teeth were carefully cleaned and were observed macroscopically. After air-drying overnight, the teeth were sputter-coated with carbon CC-40F (Meiwa-shouji, Osaka, Japan), and were observed with a Hitachi S-4000 scanning electron microscope (Hitachi Electronics, Tokyo, Japan) operated at 15 kV. For the observation of enamel rod inclination, sagittal sections of maxillary incisors were etched by a grinder for 30 seconds in 0.1N hydrochloric acid and were observed similarly.

Chemical and Mineralization Analyses

Qualitative and distributive elemental analysis was performed in sagittal sections of maxillary incisors prepared with a grinder and in the labial side of maxillary incisors with a Hitachi S-2380 scanning electron microscope (Hitachi, Tokyo, Japan) operated at 15kV and energy dispersive X-ray spectrometry (EDX).

To demonstrate the patterns of mineralization, radio transparencies of the contact microradiographs were examined as previously described.[10] Maxillary incisors were dehydrated by passage through a series of ascending concentrations of ethanol solutions and embedded in polyester resin (Rigolic, Ouken Co., Tokyo, Japan). Longitudinal labio-lingual ground sections of 100-μm thickness were prepared with a rotary diamond saw (Speadrap ML521; Maruto, Tokyo, Japan) and emery papers. Microradiographs of the ground sections were recorded on Kodak SO-181 high-resolution film (Eastman Kodak, Rochester, NY) using a cabinet X-ray apparatus (CSM-2; Softex, Tokyo, Japan) at 15 kV, 4 mA for 20 minutes. The films were developed, fixed, and observed under a light microscope.

Preparation of Tissue Sections and Immunohistochemistry

Under anesthesia with ether inhalation, intracardiac perfusions for 2-week-old mice were performed with a fixative solution containing 4% paraformaldehyde in PBS, pH 7.4. Postfixation was ensured by immersion of dissected maxilla and mandible in the fixative solution overnight at 4°C.

The maxillae and mandibles with incisors were processed for histological analysis by decalcification at 4°C for up to 2 weeks in a pH 7.4 PBS solution containing 10% EDTA. After extensive washing in PBS, the samples were dehydrated in increasing concentrations of ethanol and lemosol (Wako, Osaka, Japan), and were finally embedded in paraffin. Serial longitudinal and frontal sections of the incisors of the paraffin-embedded specimens (5 μm) were processed for H&E staining.

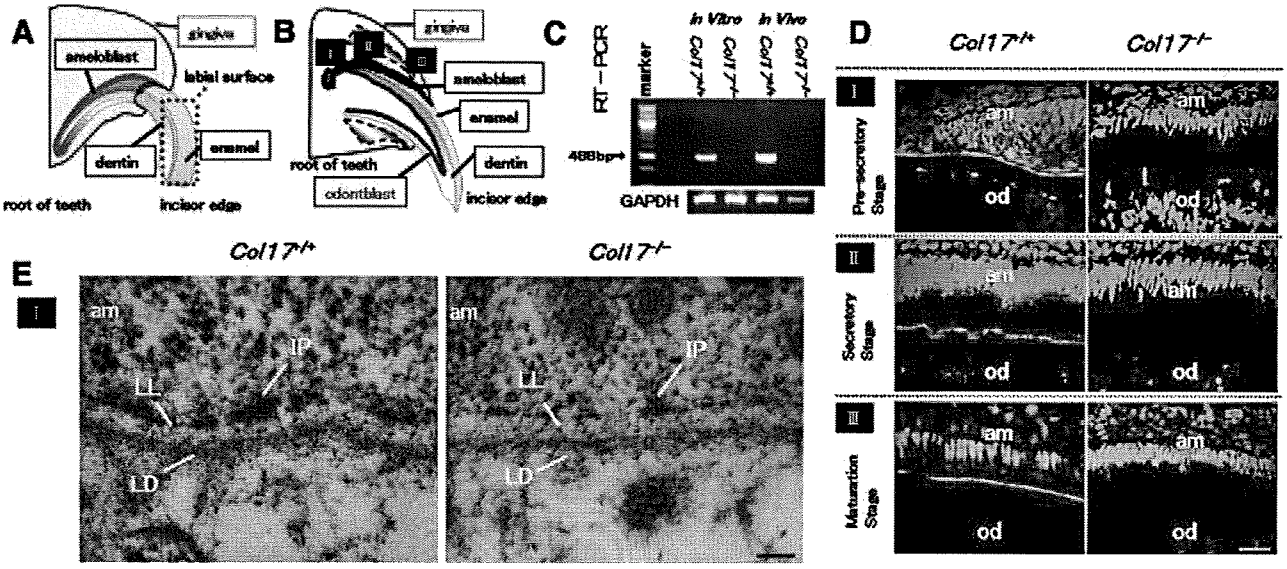

Figure 1. COL17 expression in the tooth of *Col17*$^{+/+}$ mice and COL17 absence in the tooth of *Col17*$^{-/-}$ mice. **A, B:** Mouse incisors are continuously elongating teeth. In the root of these incisors, ameloblasts (blue) and odontoblasts (green) secrete enamel matrix and dentin, respectively, during the secretory stage (II). I: the pre-secretory stage; II: the secretory stage; III: the maturation stage. **C:** A RT-PCR assay revealed that *Col17* mRNA (488 bp band) was expressed in cultured ameloblasts from *Col17*$^{+/+}$ mice (**left lane**) and *Col17*$^{+/+}$ mouse teeth (**second right**). *Col17* mRNA was not expressed in cultured ameloblasts from *Col17*$^{-/-}$ mice (**second left lane**) or *Col17*$^{-/-}$ mouse teeth (**right hand lane**). **D:** Immunofluorescence staining for COL17 (green) revealed that COL17 was expressed in the EMJ between ameloblasts and odontoblasts at the pre-secretory stage of a *Col17*$^{+/+}$ mouse (**upper, left**), between ameloblasts and enamel matrix in the secretory stage (**middle, left**) and in the maturation stage (**lower, left**) of a *Col17*$^{+/+}$ mouse. At the secretory stage, COL17 expression was weak, intermittent, or absent. In *Col17*$^{-/-}$ mice, no COL17 staining was observed in the EMJ at any stage (**right column**). am: ameloblast; od: odontblast. Scale bar = 20 μm. **E:** Ultrastructural features of the basement membrane zone at the pre-secretory stage. Normal hemidesmosomes were seen in the *Col17*$^{+/+}$ mouse (**left**), but hypoplastic, malformed hemidesmosomes were observed in the *Col17*$^{-/-}$ mice (**right**). am: ameloblast; LL: lamina lucida; IP: inner attachment plaques; LD :lamina densa. Scale bar = 60 nm.

For immunohistochemistry, neonatal mice (day-1) were sacrificed and the tissue samples were embedded in optimal cutting temperature compound (Sakura Finetechnical Co., Tokyo, Japan) for frozen sectioning. Frozen tissue sections were cut at a thickness of 6 μm sagittally until incisors were exposed, or coronally until molars were exposed. Sections were fixed with acetone for 10 minutes at −20°C, and washed in PBS, incubated with a primary antibody, anti-mouse COL17 monoclonal antibody (NC-16A, final dilution, 1:2500), at 37°C for 30 minutes. Then, the sections were incubated with a secondary antibody, fluorescein isothiocyanate (FITC)-conjugated goat anti-rat IgG (H+L; Jackson ImmunoResearch Laboratories, Suffolk, UK; final dilution, 1:50), at 37°C for 30 minutes, and incubated with 10 μg/ml of propidium iodide at 37°C for 10 minutes for nuclear counterstaining. Sections were observed under an Olympus Fluoview confocal laser-scanning microscope (Olympus, Tokyo, Japan).

Ultrastructural Analysis during Tooth Formation

As above, from the maxillomandibular tissue fixed with modified Karnovsky's fixative (at a final concentration of 2% paraformaldehyde and 2.5% glutaraldehyde in 0.05 mol/L cacodylate buffer solution, pH 7.4), 2-week-old mice incisors were obtained and decalcified in 10% EDTA pH 7.4, at 4°C for 2 weeks. After decalcification, samples were postfixed in 1% osmium tetroxide at 4°C for 2 hours and stained *en bloc* with 1% uranyl acetate at 4°C for 20 minutes. The samples were dehydrated through a graded series of ethanol and embedded in Epon 812 (TAAB Laboratories, Berkshire, UK). Ultrathin sections were cut in the sagittal direction to include both the separated enamel organ and the dental papilla. Sections were stained with uranyl acetate and lead citrate, and observed under a Hitachi H-7000 transmission electron microscope (Hitachi, Tokyo, Japan).

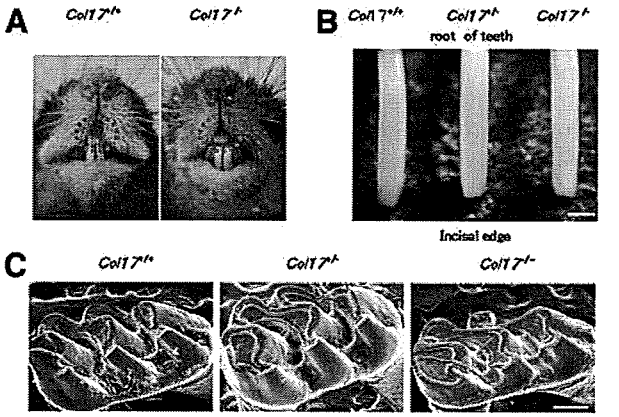

Figure 2. Dental phenotype of *Col17*$^{-/-}$ mice. **A:** At 4 weeks of age, a *Col17*$^{-/-}$ mouse (**right**) had whitish incisors. **B:** Incisors from *Col17*$^{+/+}$ and *Col17*$^{+/-}$ mice showed yellowish color, although an incisor from a *Col17*$^{-/-}$ mouse seemed whitish (**right**). Scale bar = 500 μm. **C:** In the molars, tooth wear was more advanced for the *Col17*$^{-/-}$ mice (**right**) than for the *Col17*$^{+/+}$ (**left**) and *Col17*$^{+/-}$ (**center**) mice. Scale bar = 250 μm.

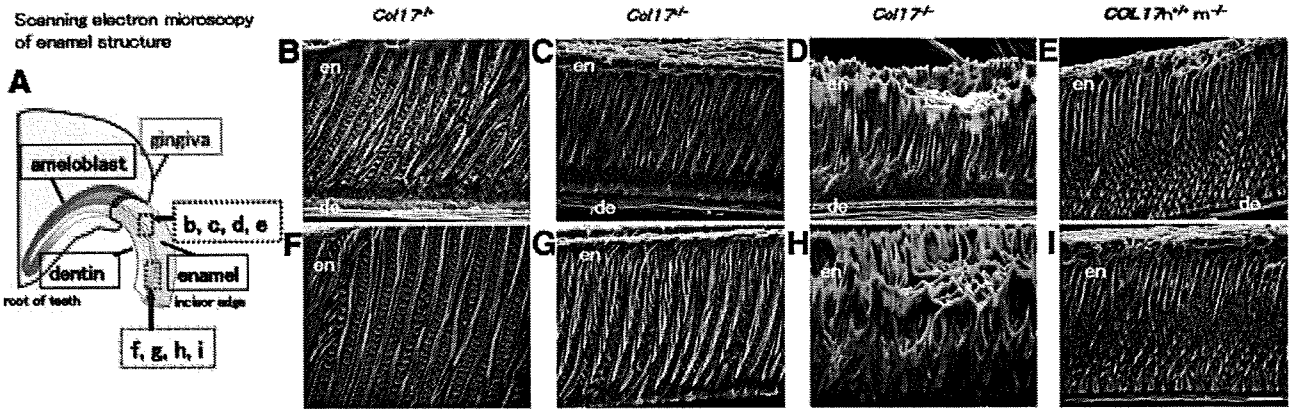

Figure 3. Scanning electron microscopy of the sagittal section of maxillary incisors. **A:** A model of an upper incisor. The enamel layer indicated by an **upper blue rectangle** and by a **lower red rectangle** is enlarged in **B**, **C**, **D** and **E**, and in **F**, **G**, **H** and **I**, respectively. In the *Col17*$^{-/-}$ mouse, irregular inclinations of enamel rods without a normal network arrangement are observed (**D**, **H**), in contrast to the regular network of enamel rods observed in the *Col17*$^{+/+}$ incisor (**B**, **F**) and in the *Col17*$^{+/-}$ incisor (**C**, **G**). The normal, regular network of enamel rods has been restored in the COL17 humanized mouse (**E**, **I**). en: enamel; de: dentin. Scale bar = 20 μm.

Terminal Deoxynucleotidyl Transferase-Mediated dUTP Nick-End Labeling Staining

For the detection of apoptotic cells in the ameloblast layer by terminal deoxynucleotidyl transferase-mediated dUTP nick-end labeling (TUNEL) assay, paraffin sections were processed with *in situ* apoptosis detection kits (Apoptag; Chemicon International, Temecula, CA).[11] The number of apoptotic ameloblasts at each stage was calculated based on the criterion that an apoptotic body of more than 2 μm in diameter could be defined as a count; these numbers were compared between *Col17*$^{+/+}$ and *Col17*$^{-/-}$.

Cell Cultures and Immunolabeling

For dental epithelial cell cultures, maxillary and mandibular incisors from 2-week-old mice were dissected, and the distal part of the incisors was removed. Tooth samples were treated with 0.25% trypsin for 10 minutes and pipetted up and down intensely. The dental epithelial cells, dental mesenchymal cells, and various other cells were isolated from incisors. To separate dental epithelial cells from the other cells, cells were cultured in epidermal keratinocyte medium containing a small amount of bovine pituitary extract (CNT-57; CELLnTEC Advanced Cell Systems, Bern, Switzerland) for 7 days. After obtaining a sufficient number of dental progenitor epithelial cells, we changed the culture medium to epidermal keratinocyte medium containing 0.07 mmol/L calcium (CNT-02; CELLnTEC Advanced Cell Systems, Bern, Switzerland) to induce differentiation, and cultured it for 10 days.

For fluorescence staining, the cells were fixed with 70% ethanol for 10 minutes and washed with PBS. The cells were incubated with a primary antibody anti-mouse amelogenin polyclonal antibody (Hokudo, Sapporo, Japan), final dilution of 1:100 or with anti-mouse ameloblastin polyclonal antibody (Santa Cruz Biotechnology, Santa Cruz, CA), final dilution, 1:50, at 37°C for 30 minutes. Then, the cells were incubated with the secondary antibody FITC-conjugated goat anti-rabbit IgG (H+L; Jackson ImmunoResearch Laboratory, West Grove, PA), final dilution, 1:50, or with FITC-conjugated donkey anti-goat IgG (H+L; Jackson ImmunoResearch Laboratory, West Grove, PA), final dilution, 1:50, at 37°C for 30 minutes and incubated with 10 μg/ml of propidium iodide at 37°C for 10 minutes to visualize the nucleus. The cells were observed under an Olympus FluoView confocal laser-scanning microscope (Olympus, Tokyo, Japan).

RT-PCR Analysis

To study *Col17* mRNA expression in dental epithelial cells and ameloblasts, total RNA from incisors or cultured dental epithelial cells was extracted using TRIZOL reagent (Invitrogen, Carlsbad, CA), according to the manufacturer's instructions. Extracted RNA was used for cDNA synthesis in SuperScript III reverse transcriptase (Invitrogen, Carlsbad, CA) according to the manufacturer's instructions. The following primers specific for mouse *Col17* sequence (NM: 007732) were used for RT-PCR: 5′-AGAAGAAAA GCATCCGAGGG-3′ (RT-F); and 5′-TGGTTGAAGAAGAGGCGAGT-3′ (RT-B). As a control, we used the primers for mouse glyceraldehyde-3-phosphate dehydrogenase (GAPDH; NM: 001001303): 5′-TTAGCCCCCCTGGCCAAGG-3′ (mGAPDH-F) and 5′-CTTACTCCTTGGAGGCCATG-3′ (mGAPDH-B), which amplified a 541-bp fragment.

Real-Time RT-PCR Analysis

To quantitatively analyze mRNA expression levels of tooth-formation-associated proteins, amelogenin, ameloblastin, enamelin, tuftelin, enamelysin, and dentin sialophosphoprotein (DSPP), in teeth from the *Col17*$^{+/+}$ and *Col17*$^{-/-}$ mice, cDNA samples were analyzed using the ABI prism 7000 sequence detection system (Applied Biosystems, Foster City, CA). Primers and probes specific for amelogenin, ameloblastin, enamelin, tuftelin, enamelysin, DSPP, and control housekeeping genes, GAPDH and β-ac-

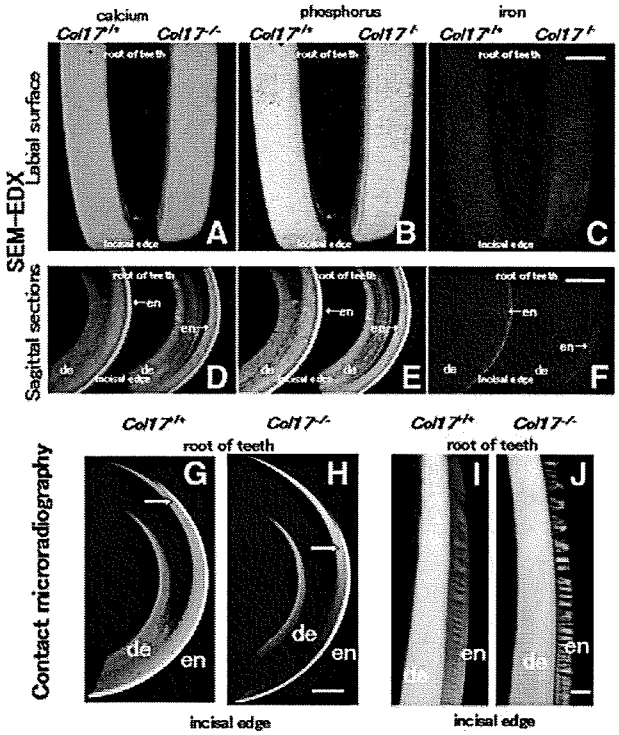

Figure 4. Difference in enamel formation between $Col17^{+/+}$ and $Col17^{-/-}$ mice incisors. The labial surface (see Figure 1A) is featured in **A**, **B**, and **C**. A sagittal section is shown in **D**, **E**, and **F**. **A, B:** The labial surface of the maxillary incisors in both $Col17^{+/+}$ (**left**) and $Col17^{-/-}$ (**right**) mice was scanned for calcium (green) and phosphorus (yellow) with EDX spectrometry. No obvious difference was observed in elemental distribution mapping. **C:** The same surfaces scanned in EDX for iron (red). In $Col17^{-/-}$ mice (**right**), the distribution of iron was irregular, compared with that of a $Col17^{+/+}$ mice (**left**). Scale bar: (**A, B, C**) = 500 μm. **D, E, F:** The sagittal sections of the maxillary incisors of both $Col17^{+/+}$ (**left**) and $Col17^{-/-}$ (**right**) mice scanned in EDX for calcium (green), phosphorus (yellow), and iron (red). No obvious difference is observed in the distribution of calcium or phosphorus between the $Col17^{+/+}$ (**left**) and $Col17^{-/-}$ (**right**) mice. In the $Col17^{-/-}$ mice (**right**), the iron concentration in the enamel is lower than that in the $Col17^{+/+}$ mouse (**left**; **F**). en: enamel; de: dentin. Scale bars in (**D, E, F**) = 1000 μm. **G, H:** Microradiographs of maxillary incisors in $Col17^{+/+}$ (**G**) and $Col17^{-/-}$ (**H**) mice. The position (**arrows**) where sufficient mineralization occurred in the enamel judged from the low radio-opacity signal, moved toward the incisal edge in maxillary incisors of a $Col17^{-/-}$ mouse (**G**), compared with that in incisors of a $Col17^{+/+}$ mouse (**H**). en: enamel; de: dentin. Scale bar: (**G, H**) = 500 μm. **I, J:** Microradiographs showing the mineralization pattern of the developing enamel at the maturation stage from $Col17^{+/+}$ (**I**) and $Col17^{-/-}$ (**J**) mice. As compared with $Col17^{+/+}$ (**I**), the mineralization demonstrated by radio-opacity of the enamel was irregular in both stages in $Col17^{-/-}$ mice (**J**), although there were no differences in the radio-opacity of dentine between $Col17^{+/+}$ (**I**) and $Col17^{-/-}$ (**J**) mice. en: enamel; de: dentin. Scale bar: (**I, J**) = 100 μm.

tin, were obtained from the TaqMan gene expression assay (Applied Biosystems, Foster City, CA; Probe ID; Mm00711644_g1, Mm00477485_m1, Mm00516922_m1, Mm00449139_m1, Mm00600244_m1 and Mm00515666_m1, Mm99999915_gl, Mm00607939_sl).

Differences between the mean CT values of mRNA expressions of tooth-formation-associated proteins and those of GAPDH or ß-actin were calculated as $\Delta CT_{Col17-/-\ mice} = CT_{tooth\ protein} - CT_{GAPDH\ (or\ other\ housekeeping\ genes)}$ and those of ΔCT for the $Col17^{+/+}$ incisors as $CT_{calibrator} = CT_{tooth\ protein} - CT_{GAPDH\ (or\ other\ housekeeping\ genes)}$. Final results for $Col17^{-/-}$ incisor samples/$Col17^{+/+}$ incisor samples (%) were determined by $2^{-(CT\ Col17-/-\ -\ CTcalibrator)}$.

Using similar methods, we quantitatively analyzed the tooth-formation-associated protein mRNA expression levels in the dental epithelial cells cultured from the $Col17^{+/+}$ and $Col17^{-/-}$ mice.

Results

COL17 Expression Pattern in the EMJ of Teeth in $Col17^{-/-}$ Mice

We observed the expression of *Col17* at each of the three stages of enamel formation: pre-secretory, secretory, and maturation (Figure 1, A and B). The 488-bp fragments of mouse *Col17* mRNA were detected in $Col17^{+/+}$ mouse incisors *in vivo* and in cells cultured from $Col17^{+/+}$ mouse incisors *in vitro*, although mouse *Col17* mRNA was detected in neither incisors nor cultured cells from $Col17^{-/-}$ mice (Figure 1C).

To clarify COL17 expression during tooth formation, we immunostained tissue sections of maxillary incisors in which we could observe all differentiation stages of tooth formation. COL17 was expressed in the EMJ between ameloblasts and odontoblasts at the pre-secretory stage. Due to elongation of Tomes' processes, the basement membrane became discontinuous and COL17 expression was reduced and in places became intermittent at the secretory stage. COL17 expression reappeared at the maturation stage (Figure 1D).

In the $Col17^{-/-}$ mice, COL17 expression was not observed in the EMJ under the ameloblasts at any stage during tooth development.

The basement membrane on the basal surface of the ameloblasts separates the ameloblasts from mesenchymal tissue/pre-odontoblasts. Hemidesmosomes are observed in the EMJ, and they are composed of prominent inner plaques, outer plaques, and sub-basal dense plates, similar to those in the dermo-epidermal junction in the skin. Anchoring filaments cross the lamina lucida, and anchoring fibrils anchor lamina densa to the mesenchymal tissue in the $Col17^{+/+}$ mice (Figure 1E).

In the $Col17^{-/-}$ mice, there were a reduced number of hypoplastic inner and outer hemidesmosomal attachment plaques with poor keratin filament association and less prominent anchoring filaments, whereas anchoring fibrils and the lamina densa were both normally preserved (Figure 1E).

Dental Phenotype in the $Col17^{-/-}$ Mice

The incisors of wild-type ($Col17^{+/+}$) and heterozygous ($Col17^{+/-}$) mice exhibit yellow pigmentation on the surface. The incisors of the $Col17^{-/-}$ mice had a chalky, whitish appearance (Figure 2, A and B). The *Col17*-rescued mice (mouse $Col17^{-/-}$, human $COL17^{+/+}$) had yellowish incisors, as did the wild-type $Col17^{+/+}$ mice (data not shown). By scanning electron microscopy, the enamel surface of the $Col17^{+/+}$, $Col17^{+/-}$ and $Col17^{-/-}$ mice appeared smooth and unpitted (data not shown). Molar wear was more advanced in the $Col17^{-/-}$ mice than in the $Col17^{+/+}$ and $Col17^{+/-}$ mice. This tooth wear

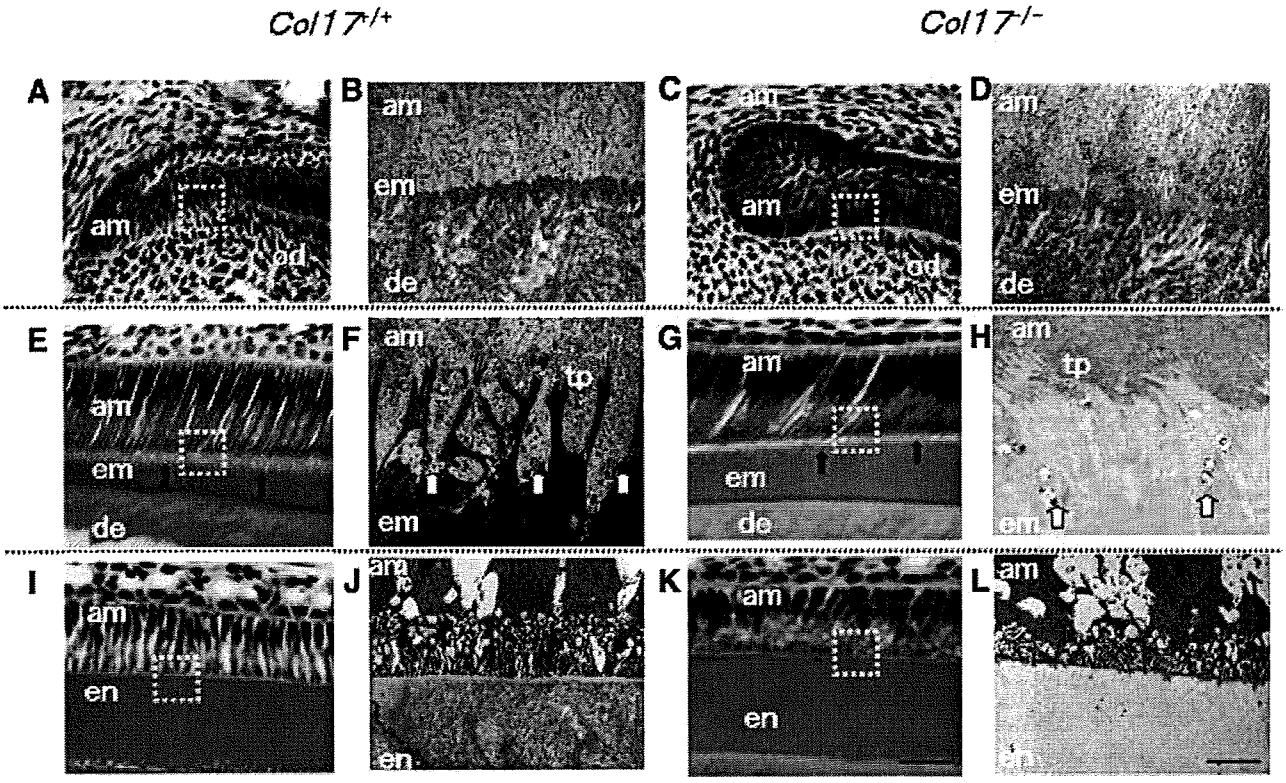

Figure 5. Malformed Tomes' processes and defective amelogenesis in *Col17*$^{-/-}$ mice **A–D:** At the pre-secretory and early secretory stages, the EMJ separates pre-ameloblasts and pre-odontoblasts. **A, C:** The overall structures of pre-ameloblasts and pre-odontoblasts were similar in the *Col17*$^{+/+}$ **(A)** and *Col17*$^{-/-}$ **(C)** mice in the pre-secretory to the early secretory stages at the light microscopic level. **B, D:** Ultrastructurally, from the pre-secretory to the early secretory stages, the basement membrane between ameloblasts and odontoblasts was blurred in the *Col17*$^{-/-}$ mouse **(D)**, compared with more obvious, intact basement membrane structures in a *Col17*$^{+/+}$ mouse **(B)**. **E–H:** At the secretory stage, Tomes' processes are formed and enamel matrix is produced by ameloblasts. **E, G:** In the secretory stage, the processes of ameloblasts were malformed and blurred **(arrows)** in the *Col17*$^{-/-}$ mouse **(G)**, compared with well-organized lattice-like structures of the Tomes' processes **(arrows)** in the *Col17*$^{+/+}$ mice **(E)**. The thickness of the enamel matrix seemed similar both in *Col17*$^{+/+}$ **(E)** and *Col17*$^{-/-}$ **(G)** mice. At the secretory stage, Tomes' processes were apparently hypoplastic in the *Col17*$^{-/-}$ mouse **(H)**, compared with normal Tomes' processes in the *Col17*$^{+/+}$ mouse **(F)**. **I–L:** In the maturation stage, disruption of the processes of ameloblasts (am) was more advanced in the *Col17*$^{-/-}$ mouse **(K)**, compared with regular processes in the *Col17*$^{+/+}$ mice **(I)**. At the maturation stage, the electron density of the enamel matrix is remarkably lower in the *Col17*$^{-/-}$ mouse **(L)** than that in the *Col17*$^{+/+}$ mouse **(J)**. In addition, enamel rod structures are blurred in the enamel matrix of the *Col17*$^{-/-}$ mouse **(L)**. am: ameloblast; em: enamel matrix; en: enamel; de: dentin; od: odontoblast; tp: Tomes' processes. Scale bars: **(A, C, E, G, I, K)** = 30 μm; **(B, D, F, H, J, L)** = 3 μm.

became more severe with age, although it failed to extend to loosen the molar crown (Figure 2C). In sagittal sections of the *Col17*$^{-/-}$ mice maxillary incisors, the enamel rod inclination was irregularly oriented and disrupted and had lost its normal network arrangement seen in that of *Col17*$^{+/+}$ and *Col17*$^{+/-}$ mice (Figure 3 A–D, F–H). In the COL17-rescued mouse *Col17*$^{-/-}$, human *COL17*$^{+/+}$ mice, the maxillary incisors showed normal enamel rod formation (Figure 3, E and I) confirming that the enamel changes were caused by a Col17 deficiency.

Chemical and Mineralization Analysis of the Teeth

Backscatter electron images of the labial surface and the sagittal sections of the maxillary incisors in the *Col17*$^{+/+}$, *Col17*$^{+/-}$, and *Col17*$^{-/-}$ mice revealed that calcium and phosphorus were homogeneously distributed from incisal edge to apical root in all samples (Figure 4A, B, D, E). In the *Col17*$^{+/+}$ and *Col17*$^{+/-}$ mice, iron was lightly but uniformly distributed from incisal edge to the middle of teeth, and the density corresponded with the yellow pigmentation. In the *Col17*$^{-/-}$ mice, iron was irregularly distributed (Figure 4, C and F).

To compare the mineralization patterns of teeth between the *Col17*$^{+/+}$ and *Col17*$^{-/-}$ mice, radio transparencies of the microradiographs were examined in maxillary incisors. The radio-opacity of enamel decreased gradually toward the incisal edge, from the enamel secretory stage to the maturation stage. Mineralization reached its maximum during the late maturation stage (Figure 4G). To objectively evaluate the mineralization level in the enamel layers, we set up a marker-point for enamel matrix sufficiently completed mineralization using image analysis. The point exhibited 90% or more saturation levels in the completely mineralized incisal edge-side of enamel layer. We then assessed each image for the area that showed this or higher saturation signals. The mineralization marker-points that we defined were at 1.7 mm and 2.7 mm from the incisor root in the *Col17*$^{+/+}$ mice and *Col17*$^{-/-}$ mice, respectively (Figure 4H). These findings indicated that, in the *Col17*$^{-/-}$ incisors, mineralization of enamel was delayed by 1.0 mm toward the incisal edge compared with that of the

Col17$^{+/+}$ incisors. Mineralization of the enamel matrix, at the maturation stage, was irregular and discontinuous in the *Col17*$^{-/-}$ mice (Figure 4I) compared with the *Col17*$^{+/+}$ mice (Figure 4J).

Defective Amelogenesis in Col17$^{-/-}$ *Mice*

Ameloblast size and the enamel matrix thickness in the *Col17*$^{-/-}$ mice were similar to those in the *Col17*$^{+/+}$ mice. The Tomes' processes of the *Col17*$^{+/+}$ mice were triangular and arranged in order. However, the processes of the *Col17*$^{-/-}$ mice were deformed and difficult to clearly visualize in H&E-stained sections (Figure 5A, C, E, G, I, K).

Furthermore, we observed enamel formation of the incisors of the *Col17*$^{+/+}$, *Col17*$^{+/-}$, and *Col17*$^{-/-}$ mice ultrastructurally. Secretory ameloblasts were tall columnar cells with intact Tomes' processes producing enamel matrix in the *Col17*$^{+/+}$ and *Col17*$^{+/-}$ mice (Figure 5, B and D).

In the *Col17*$^{-/-}$ mice, the Tomes' processes were thin, fragmented and disorganized, showing a wavy, villous appearance. There was no obvious difference in the other structural components of the ameloblasts (Figure 5, F and H).

Mature ameloblasts were columnar cells and could be divided into ruffle-based ameloblasts and smooth-ended ameloblasts by the presence of a ruffled border. Rough endoplasmic reticulum, lysosomes, mitochondria, small vacuoles and Golgi apparatus were seen in the apical and mid portions of mature ameloblasts. The cell structure and organelles of *Col17*$^{-/-}$ mature ameloblasts appeared normal, but the enamel rods were malformed and irregularly distributed. The electron density of the enamel matrix was remarkably low during the secretory and maturation stages in the *Col17*$^{-/-}$ mice, compared with the high electron density of the enamel matrix in the *Col17*$^{+/+}$ and *Col17*$^{+/-}$ mice (Figure 5, J and L).

Assay of Ameloblast Proliferation and Differentiation

Colony-forming analysis revealed there was no significant difference in colony-forming ability of cultured ameloblasts between the Col17$^{+/+}$ and Col17$^{-/-}$ mice (data not shown). As for apoptosis, TUNEL staining did not reveal excessive apoptosis of ameloblasts at the pre-secretory to secretory stages in either the Col17$^{+/+}$ or the Col17$^{-/-}$ mice (data not shown).

TUNEL assays showed that some apoptotic cells appeared from the late secretory stage to the early maturation stage (called the "transitional stage") of the *Col17*$^{+/+}$ and *Col17*$^{-/-}$ mice (data not shown). However, there was no significant difference in the number of TUNEL-positive cells between *Col17*$^{+/+}$ and *Col17*$^{-/-}$ mice; in the numbers of apoptotic ameloblasts per sagittal incisor section, 7.5 ± 0.7 cells/sagittal section in *Col17*$^{+/+}$ incisors and 7.0 ± 1.0 cells/sagittal section in *Col17*$^{-/-}$ incisors.

We examined the expression of enamel proteins in the incisors *in vivo* and in cultured dental epithelial cells *in vitro* using real-time RT-PCR analysis.[12–14] mRNA expression of the major enamel proteins produced by ameloblasts, including amelogenin, ameloblastin, enamelin, enamelysin, and DSPP, was significantly decreased in the *Col17*$^{-/-}$ incisors, except for the expression of tuftelin (Figure 6A). Tuftelin expression was only slightly reduced in *Col17*$^{-/-}$ mice incisors. In dental epithelial cells cultured from the *Col17*$^{+/+}$ mice, mRNA expression of amelogenin, ameloblastin, enamelin, and tuftelin was confirmed, although mRNA expression of enamelysin and DSPP was absent. In the *Col17*$^{-/-}$ mice, mRNA expression of amelogenin, ameloblastin and enamelin in cultured cells were remarkably lower than in the *Col17*$^{+/+}$ mice. Tuftelin expression was higher than that in the cells cultured from the *Col17*$^{+/+}$ mice (Figure 6B). Immunocy-

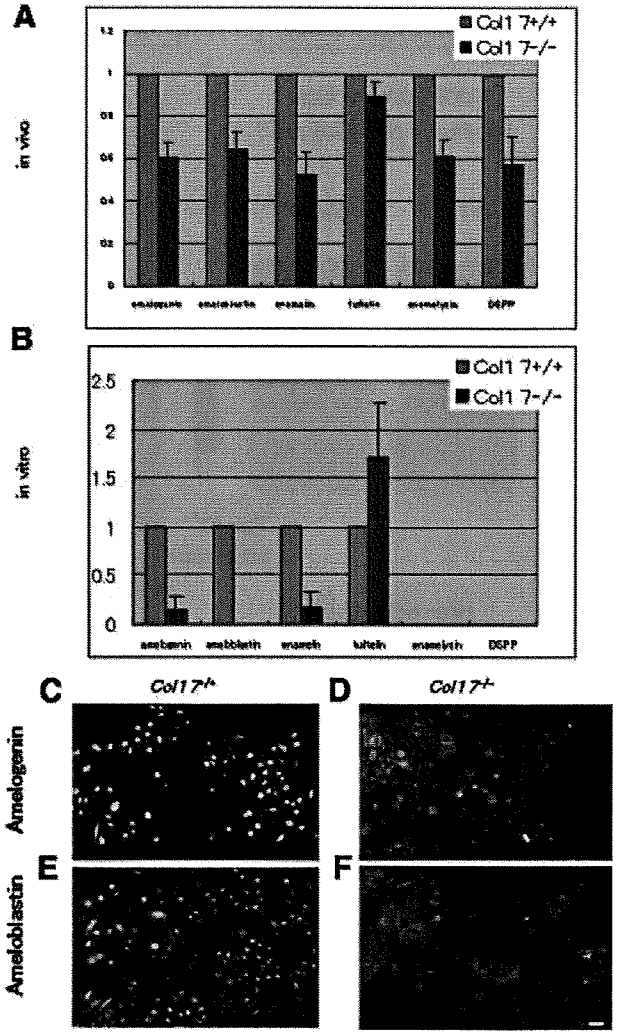

Figure 6. Expression of enamel proteins in *Col17*$^{-/-}$ ameloblasts. **A:** mRNA expression of all of the enamel proteins examined (amelogenin, ameloblastin, enamelin, tuftelin, enamelysin, and DSPP) was down-regulated in ameloblasts of incisors of the *Col17*$^{-/-}$mice *in vivo*. **B:** *In vitro* ameloblasts cultured from incisors of the *Col17*$^{-/-}$ mice showed down-regulated mRNA expression of amelogenin, ameloblastin and enamelin, although tuftelin expression was up-regulated relative to tuftelin expression of the cultured ameloblasts from the *Col17*$^{+/+}$ mice. Neither enamelysis nor DSPP was expressed in ameloblasts cultured from the *Col17*$^{+/+}$ and *Col17*$^{-/-}$ mice. **C:** Protein expression (FITC, green) of amelogenin and ameloblastin was decreased in ameloblasts cultured from the *Col17*$^{-/-}$ mice (**D, F**), relative to that in ameloblasts cultured from the *Col17*$^{+/+}$ mice (**C, E**). (**C, D**) amelogenin staining; (**E, F**) ameloblastin staining; (**C, E**) cells from *Col17*$^{+/+}$ mice; (**D, F**) cells from *Col17*$^{-/-}$ mice. Scale bar = 20 μm.

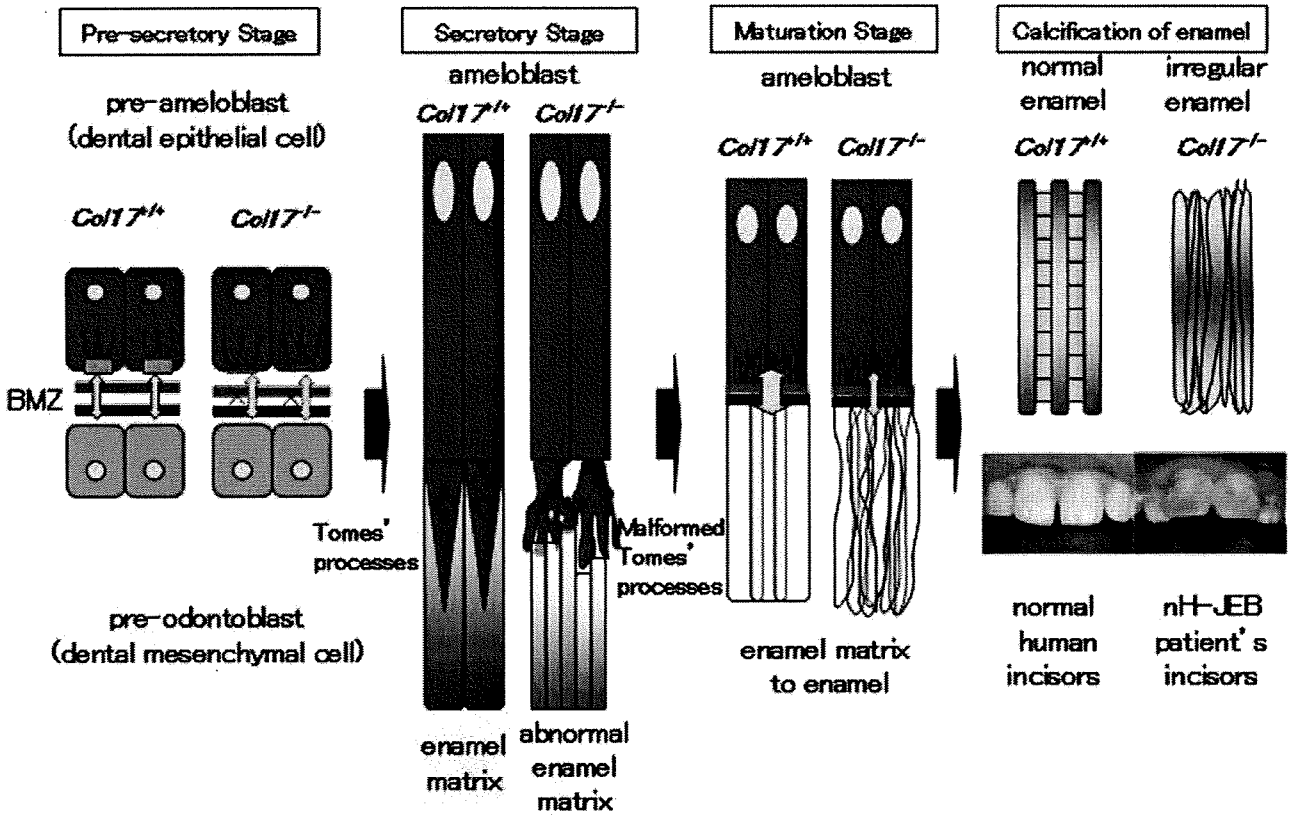

Figure 7. Schemes of normal enamel formation in *Col17*$^{+/+}$ mice and defective enamel formation in *Col17*$^{-/-}$ mice. In the *Col17*$^{+/+}$ incisors (**left**), normal enamel matrix is formed by Tomes' processes, resulting in intact enamel formation. In the *Col17*$^{-/-}$ incisors (**right**), disruptive Tomes' processes produce disturbed enamel matrix, leading to irregular enamel formation.

tologically, strong expression of amelogenin and ameloblastin was seen in the ameloblasts cultured from the *Col17*$^{+/+}$ mice, although expression of both proteins was remarkably weak in cells cultured from the *Col17*$^{-/-}$ mice (Figure 6, C–F).

Discussion

nH-JEB is a hereditary blistering skin disease with tissue separation occurring within the lamina lucida of the epidermal basement membrane zone. nH-JEB is characterized by generalized blistering, alopecia, reduced axillary and public hair, dystrophic nails, and dental abnormalities.[4,15] Molecular genetic studies revealed that nH-JEB is caused by mutations in the genes encoding COL17 or laminin 332.[16] Most nH-JEB patients exhibit enamel hypoplasia, and pitting and coarsening of the tooth surface enamel.[6,7]

The present study revealed that the secretory ameloblasts of the *Col17*$^{-/-}$ mice lacked Tomes' processes and exhibited disturbed enamel matrix secretion, which resulted in imperfect amelogenesis demonstrated by malformed enamel rods and irregular enamel matrix (Figure 7).

Mice only have one set of dentition whereas the human disease nH-JEB affects both primary and secondary dentition. Due to these differences, the tooth abnormalities demonstrated in *Col17*$^{-/-}$ mice are unlikely to be pathophysiologically relevant to the nH-JEB human disease. However, the physiological processes of enamel formation are identical both in human and mouse dentition.[17,18] Thus, we believe that the present *Col17*$^{-/-}$ mice are a practical and useful model in which to study nH-JEB dental abnormalities.

We studied the developmental processes of the teeth in *Col17*$^{-/-}$ mice. The teeth develop through the presecretory, secretory, and maturation stages.[19] At presecretory stage, hypoplasia of hemidesmosomes is the only apparent abnormality in *Col17*$^{-/-}$ mice teeth. In ameloblasts in the secretory stage, disturbed Tomes' process formation was observed in the *Col17*$^{-/-}$ mice, although enamel matrix was seen around the disrupted Tomes' processes. The Tomes' processes are known to be involved in the secretion of enamel matrix.[19]

Ameloblasts at the maturation stage showed no apparent abnormality, although the crystal structure of the enamel matrix was disturbed in the *Col17*$^{-/-}$ mice. Scanning electron microscopy revealed that enamel rods were malformed and irregular in the enamel matrix of the *Col17*$^{-/-}$ mice. These morphological abnormalities were not observed in the rescued COL17-humanized mice and thus it was confirmed that the abnormalities were direct effects of the COL17 deficiency.

Contact microradiography demonstrated that enamelization of the enamel matrix and calcification were delayed in the *Col17*$^{-/-}$ mice. In addition, reduced iron